

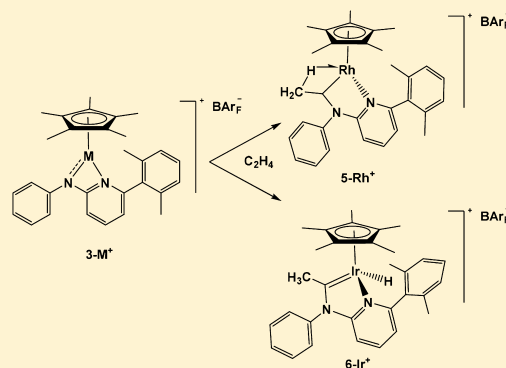
# Activation of Small Molecules by the Metal–Amido Bond of Rhodium(III) and Iridium(III) ( $\eta^5$ -C<sub>5</sub>Me<sub>5</sub>)M–Aminopyridinate Complexes

Ana Zamorano, Nuria Rendón,\*<sup>1b</sup> Joaquín López-Serrano,<sup>1b</sup> Eleuterio Álvarez, and Ernesto Carmona

Instituto de Investigaciones Químicas (IIQ), Departamento de Química Inorgánica and Centro de Innovación en Química Avanzada (ORFEO-CINQA), Universidad de Sevilla and Consejo Superior de Investigaciones Científicas (CSIC), Avenida Américo Vespucio 49, 41092 Sevilla, Spain

## S Supporting Information

**ABSTRACT:** We report the synthesis and structural characterization of five-coordinate complexes of rhodium and iridium of the type  $[(\eta^5\text{-C}_5\text{Me}_5)\text{M}(\text{N}^{\wedge}\text{N})]^+$  (**3-M<sup>+</sup>**), where N<sup>∧</sup>N represents the aminopyridinate ligand derived from 2-NH(Ph)-6-(Xyl)C<sub>5</sub>H<sub>3</sub>N (Xyl = 2,6-Me<sub>2</sub>C<sub>6</sub>H<sub>3</sub>). The two complexes were isolated as salts of the BAR<sub>F</sub><sup>−</sup> anion (BAR<sub>F</sub><sup>−</sup> = B[3,5-(CF<sub>3</sub>)<sub>2</sub>C<sub>6</sub>H<sub>3</sub>]<sub>4</sub>). The M–N<sub>amido</sub> bond of complexes **3-M<sup>+</sup>** readily activated CO, C<sub>2</sub>H<sub>4</sub>, and H<sub>2</sub>. Thus, compounds **3-M<sup>+</sup>** reacted with CO under ambient conditions, but whereas for **3-Rh<sup>+</sup>**, CO migratory insertion was fast, yielding a carbamoyl carbonyl species, **4-Rh<sup>+</sup>**, the stronger Ir–N<sub>amido</sub> bond of complex **3-Ir<sup>+</sup>** caused the reaction to stop at the CO coordination stage. In contrast, **3-Ir<sup>+</sup>** reacted reversibly with C<sub>2</sub>H<sub>4</sub>, forming adduct **5-Ir<sup>+</sup>**, which subsequently rearranged irreversibly to [Ir](H)(=C(Me)N(Ph)–) complex **6-Ir<sup>+</sup>**, which contains an N-stabilized carbene ligand. Computational studies supported a migratory insertion mechanism, giving first a  $\beta$ -stabilized linear alkyl unit, [Ir]CH<sub>2</sub>CH<sub>2</sub>N(Ph)–, followed by a multistep rearrangement that led to the final product **6-Ir<sup>+</sup>**. Both  $\beta$ - and  $\alpha$ -H eliminations, as well as their microscopic reverse migratory insertion reactions, were implicated in the alkyl-to-hydride–carbene reorganization. The analogous reaction of **3-Rh<sup>+</sup>** with C<sub>2</sub>H<sub>4</sub> originated a complex mixture of products from which only a branched alkyl [Rh]C(H)(Me)N(Ph)– (**5-Rh<sup>+</sup>**) could be isolated, featuring a  $\beta$ -agostic methyl interaction. Reactions of **3-M<sup>+</sup>** with H<sub>2</sub> promoted a catalytic isomerization of the Ap ligand from classical  $\kappa^2$ -N,N' binding to  $\kappa$ -N plus  $\eta^3$ -pseudoallyl coordination mode.



## INTRODUCTION

In recent years, we have explored the chemistry of cationic  $[(\eta^5\text{-C}_5\text{Me}_5)\text{M}^{\text{III}}]$  complexes of rhodium and iridium stabilized by coordination to bulky, formally monoanionic bidentate ligands (L<sup>−</sup>X), encompassing cyclometalated phosphines and, especially in the context of this work, aminopyridinates.<sup>1,2</sup> The latter are also called pyridylamido ligands and are represented onward in a simplified manner as Ap or as N<sup>∧</sup>N (see Figure 1).<sup>3</sup> Compounds built around  $[(\eta^5\text{-C}_5\text{Me}_5)\text{M}]$  rhodium and iridium frameworks have arisen considerable interest because they are valuable molecules finding countless applications in catalysis,<sup>4–7</sup> bioorganometallic studies,<sup>8,9</sup> and other areas of research.<sup>10</sup>

Similar to previously reported amido complexes of late transition metals,<sup>11</sup> the amido nitrogen atom of metal-bound aminopyridinate groups can function as a  $\pi$  donor (Figure 1a), partially offsetting the electronic unsaturation of positively charged metal centers and allowing stabilization of five-coordinate complexes of the type  $[(\eta^5\text{-C}_5\text{Me}_5)\text{M}(\text{N}^{\wedge}\text{N})]^+$ . As represented in Figure 1, bulky aryl substituents on both the amido and six positions of the pyridine termini may provide desirable steric protection to the low-coordinate metal center.

The previously reported complexes<sup>1,2</sup> behaved as markedly reactive Lewis acids upon treatment with a variety of Lewis bases

(L), forming readily the corresponding six-coordinate, 18-electron adducts  $[(\eta^5\text{-C}_5\text{Me}_5)\text{M}(\text{N}^{\wedge}\text{N})(\text{L})]^+$  (L = NH<sub>3</sub>, NCM<sub>2</sub>, CNXyl, and others). Intriguingly, none of the compounds investigated reacted with C<sub>2</sub>H<sub>4</sub> even under rather forcing conditions, hampering the observation of products originating from migratory insertion of the alkene into the M–N<sub>amido</sub> bond.<sup>12,13</sup> It appeared plausible that failure to detect C<sub>2</sub>H<sub>4</sub> reactivity was due to steric reasons, in other words, that the required side-on metal approach of the C=C bond was impeded by steric interactions with the C<sub>5</sub>Me<sub>5</sub> and Ap ligands, in particular with the aryl substituents of the amido nitrogen atom. In accordance with this assumption, it was found that complexes of rhodium and iridium alike exhibited a significant decrease in the rate of H<sub>2</sub>-catalyzed isomerization of the coordinated pyridylamido ligand from the common  $\kappa^2$ -N,N' binding to an unconventional  $\kappa$ -N, $\eta^3$ -benzylic binding mode (Figure 1b), when the amido nitrogen substituent was changed from 2,6-Me<sub>2</sub>C<sub>6</sub>H<sub>3</sub> to 2,6-Pr<sub>2</sub>C<sub>6</sub>H<sub>3</sub>.

Considering the above information, we deemed of interest studying the chemistry of related  $[(\eta^5\text{-C}_5\text{Me}_5)\text{M}(\text{N}^{\wedge}\text{N})]^+$

Received: September 6, 2017

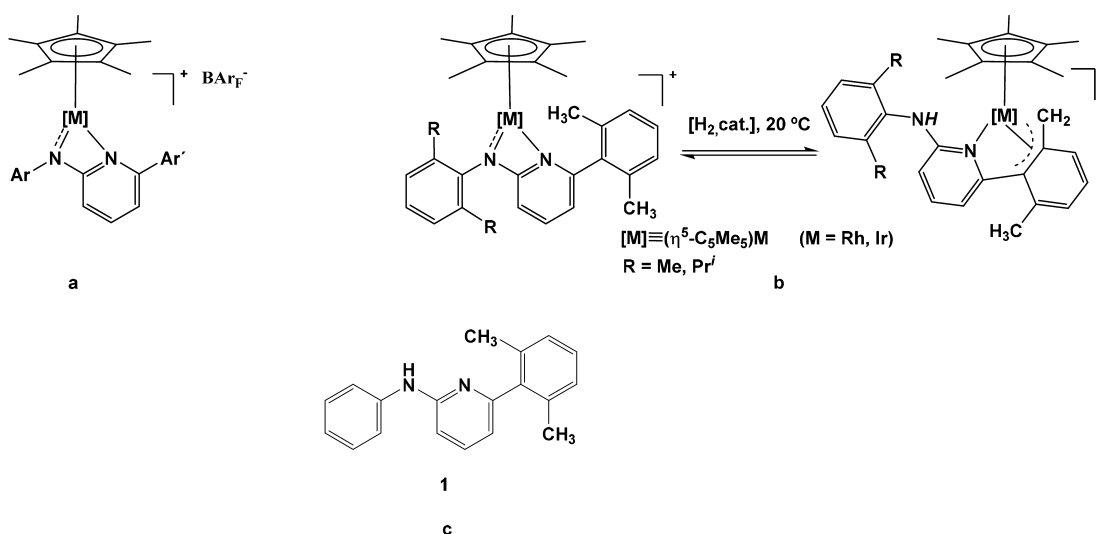


**Figure 1.** (a) General representation for five-coordinate complexes of  $[(\eta^5\text{-C}_5\text{Me}_5)\text{M}^{\text{III}}]^+$  units ( $M = \text{Rh, Ir}$ ) and aryl-substituted aminopyridinate ligands. (b) Previously reported  $\text{H}_2$ -catalyzed isomerization of the Ap ligand of complexes of type a. (c) Aminopyridinate precursor, **1**, utilized in this work.

complexes,  $3\text{-Rh}^+$  and  $3\text{-Ir}^+$ , in which the aminopyridinate ligand is the conjugated base of phenyl[6-(2,6-dimethylphenyl)pyridin-2-yl]amine (compound **1** in Figure 1c). Relative to previously assayed Ap ligands, little if any relevant changes are introduced in the overall electronic properties of the  $\text{N}^{\wedge}\text{N}$  chelating unit, whereas replacing the amido nitrogen 2,6- $\text{R}_2\text{C}_6\text{H}_3$  ( $R = \text{Me, Pr}^i$ ) substituent by the substituent-devoid phenyl group is expected to significantly mitigate steric hindrance in the vicinity of the short  $\text{M}\text{-N}_{\text{amido}}$  bond of complexes  $3\text{-M}^+$ , facilitating ligand coordination.

In this contribution, we report studies on the reactivity of complexes  $3\text{-M}^+$  toward  $\text{C}_2\text{H}_4$  that proceeds under mild conditions, yielding products stemming from migratory insertion of the olefin into the  $\text{M}\text{-N}_{\text{amido}}$  bond.<sup>12,13</sup> Computational studies supporting a mechanistic path entailing irreversible C–N bond formation, along with reversible  $\alpha$ - and  $\beta$ -H eliminations and their microscopic reverse migratory insertion reactions, are also incorporated.<sup>14</sup> Furthermore, for the investigated reaction of  $3\text{-Ir}^+$  with  $\text{C}_2\text{H}_4$ , formation of the experimentally observed hydride–carbene product **6**- $\text{Ir}^+$  was computed to be more favorable than generation of the alternative hydride–olefin isomer. The mentioned reactivity adds to the observation of CO migratory insertion into the  $\text{Rh}\text{-N}_{\text{amido}}$  bond of  $3\text{-Rh}^+$  and to the diverse and unusual H–H, C–H, and N–H bond activation encountered in the reactions of  $\text{H}_2$  with complexes  $3\text{-M}^+$ , although the latter activations are predictable on the basis of previous work.<sup>1,2</sup>

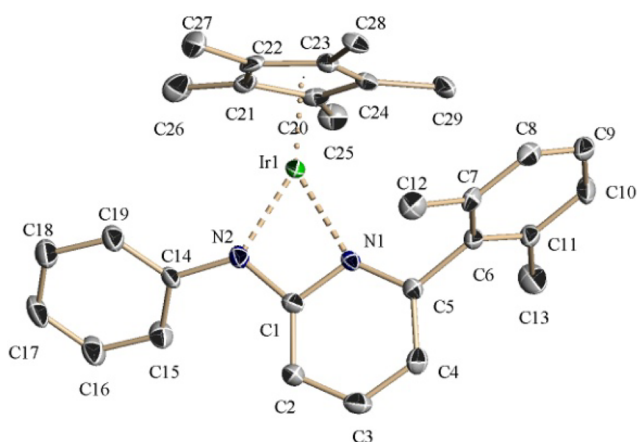
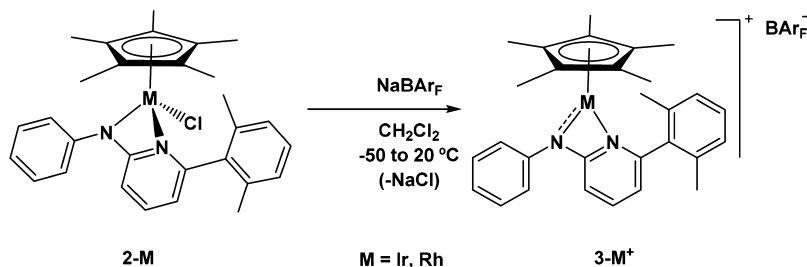
## RESULTS AND DISCUSSION

**Cationic Rhodium and Iridium  $[(\eta^5\text{-C}_5\text{Me}_5)\text{M}(\text{Ap})]^+$  Complexes.** Synthesis of the amine ligand precursor ApH (compound **1**; Figure 1c) was performed as reported previously for analogous, differently substituted aminopyridines.<sup>15</sup> Synthetic and characterization details can be found in Scheme S1. The neutral chloride complexes  $[(\eta^5\text{-C}_5\text{Me}_5)\text{M}(\text{Cl})(\text{Ap})]$  (**2-Ir** and **2-Rh**) were obtained from the corresponding  $[(\eta^5\text{-C}_5\text{Me}_5)\text{-MCl}_2]_2$  dimers and the lithium amide, LiAp. As shown in Scheme 1, the chloride ligand of compounds **2-M** was readily extruded by the action of  $\text{NaBAR}_F$  ( $\text{BAR}_F = \text{B}[3,5\text{-(CF}_3)_2\text{C}_6\text{H}_3]_4$ ) to give the five-coordinate amidopyridine complexes  $[(\eta^5\text{-C}_5\text{Me}_5)\text{-M}(\text{N}^{\wedge}\text{N})]^+$  (**3-Ir**<sup>+</sup> and **3-Rh**<sup>+</sup>). The reactions were accompanied

by a pronounced color change from the original yellow or reddish to almost black or dark brown for Ir and Rh, respectively. As noted previously,<sup>1,2</sup> the dark color of these complexes is typical of compounds of this kind in which the  $\text{M}\text{-N}_{\text{amido}}$  functionality has multiple-bond character because of  $\sigma$  and  $\pi$  donation from the anionic nitrogen atom.<sup>10,15</sup>

The four complexes **2-M** and  $3\text{-M}^+$  ( $M = \text{Rh, Ir}$ ) were fully characterized by microanalysis, IR, and multinuclear 1D and 2D NMR spectroscopy (see the Experimental Section and Supporting Information). In addition, neutral compounds **2-M**, as well as  $3\text{-Ir}^+$ , were structurally authenticated by single-crystal X-ray diffraction (XRD) studies. Figure 2 depicts the molecular structure of  $3\text{-Ir}^+$ , while those of the chloride derivatives **2-M** (Ir and Rh) are collected in Figures S35–S36. Metrical parameters have normal values, although it is worth remarking that the  $\text{Ir}\text{-N}_{\text{amido}}$  bond length of this complex (Ir1–N2 in Figure 2) at 1.972(6) Å is significantly shorter than the corresponding bond in the neutral chloride precursor **2-Ir** [2.092(2) Å], in agreement with the proposed  $\pi$ -donor nature of the amido nitrogen function of  $3\text{-Ir}^+$ . Besides, the Ir1–N2 bond is also significantly shorter than the dative covalent Ir1–N1 bond to the pyridine moiety [2.109(6) Å].

**Reactions of Complexes  $3\text{-M}^+$  with CO and  $\text{C}_2\text{H}_4$ .** Similar to related complexes of diversely substituted Ap ligands,<sup>1,2</sup> the rhodium and iridium derivatives  $3\text{-M}^+$  exhibited distinct behavior toward CO (Scheme 2). Thus, the room temperature reaction of  $3\text{-Ir}^+$  afforded the carbonyl adduct **4-Ir**<sup>+</sup>, characterized by an IR absorption at 2048  $\text{cm}^{-1}$  due to stretching of the iridium-bound C–O bond. Under the reaction conditions (Scheme 2), migratory insertion of CO into the  $\text{Ir}\text{-N}_{\text{amido}}$  bond did not take place. In contrast, an analogous CO adduct was not detected for rhodium because nucleophilic attack of the  $\text{Rh}\text{-N}_{\text{amido}}$  bond to the coordinated carbonyl occurred very rapidly with formation of a five-membered chelating carbamoylpyridine group that became stabilized by coordination of a second molecule of CO, giving the isolated complex **4-Rh**<sup>+</sup>. The incorporated CO units of this derivative gave rise to IR bands at 2077  $\text{cm}^{-1}$  (Rh–CO) and 1687  $\text{cm}^{-1}$  [Rh–C(O)N], along with corresponding <sup>13</sup>C NMR resonances with 187.1 and 189.3 ppm (<sup>1</sup> $J_{\text{CRh}} = 76$  and 30 Hz), respectively. Although not unprecedented, the insertion of CO

Scheme 1. Synthesis of the Cationic Complexes 3-M<sup>+</sup>

**Figure 2.** X-ray structure of complex 3-Ir<sup>+</sup> (30% ellipsoids, anion BARF<sup>-</sup>, and hydrogen atoms are omitted for clarity). Selected bond lengths (Å) and angles (deg): Ir1–N1 2.109(6), Ir1–N2 1.972(6), Ir1–C22 2.158(7), Ir1–C23 2.176(7), Ir1–C20 2.133(8), Ir1–C24 2.194(7), Ir1–C21 2.155(7); N2–Ir1–N1 64.3(2), C1–N1–Ir1 93.2(4), C1–N2–Ir1 98.2(4), N1–C1–N2 104.3(6).

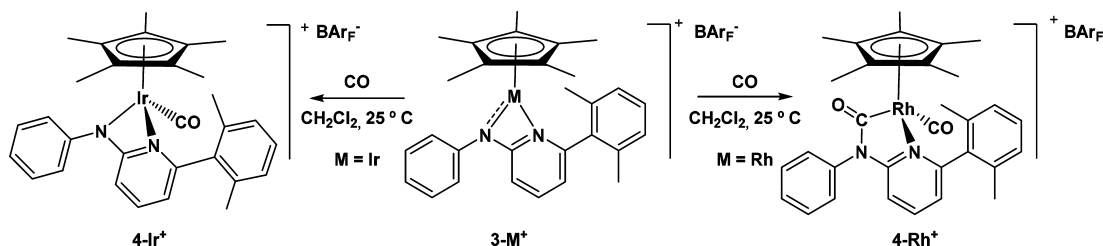
into a late-transition-metal–amide bond is a rather uncommon reaction.<sup>2,16</sup> It seems probable that the stronger third-row metal–N<sub>amido</sub> bond, relative to the Rh–N<sub>amido</sub> bond, retards migratory insertion of CO, preventing observation of the analogous iridium–carboxamide linkage. In this regard, it is worth remarking that migratory insertion of CO into the M–CH<sub>3</sub> bond of the two different systems, *fac*-[M(CH<sub>3</sub>)(I)<sub>3</sub>(CO)<sub>2</sub>]<sup>-</sup> and [(η<sup>5</sup>-C<sub>5</sub>Me<sub>5</sub>)M(Me)Cl(CO)], is 5 or 6 orders of magnitude faster on rhodium than on iridium.<sup>17</sup>

The carbonyl derivatives 4-M<sup>+</sup> were also characterized by single-crystal XRD studies. Figure 3 contains ORTEP perspective views of the molecules of the two compounds. Some relevant bond distances and angles are also given. Besides the noticeable, although expected, increase in the length of the Ir–N<sub>amido</sub> bond of 4-Ir<sup>+</sup>, now devoid of π components, relative to 3-Ir<sup>+</sup> [2.089(6) vs 1.972(6) Å], metrical parameters have normal values.

As was already recalled, the reported [(η<sup>5</sup>-C<sub>5</sub>Me<sub>5</sub>)M(N<sup>^</sup>N)]<sup>+</sup> iridium and rhodium complexes analogous to 3-M<sup>+</sup> (Figure 1b) were unreactive against C<sub>2</sub>H<sub>4</sub> (1 bar, room temperature to 130 °C). Alkenes react readily with M–H and M–C bonds through migratory insertion, a fundamental reaction in organotransition metal chemistry, key to a large number of stoichiometric and catalytic transformations.<sup>10</sup> In marked contrast, the analogous reaction of an olefin with the M–N bond of an isolated metal–amido complex to generate a new C–N bond is a less well-established transformation, with the first examples having been reported in recent years.<sup>12,13</sup>

When an ethylene atmosphere (1 bar) was introduced in a Young NMR tube containing a CD<sub>2</sub>Cl<sub>2</sub> solution of 3-Ir<sup>+</sup>, an immediate color change from almost black to orange took place, hinting at the formation of the desired C<sub>2</sub>H<sub>4</sub> adduct [(η<sup>5</sup>-C<sub>5</sub>Me<sub>5</sub>)Ir(N<sup>^</sup>N)(C<sub>2</sub>H<sub>4</sub>)]<sup>+</sup> (5-Ir<sup>+</sup>), with the structure shown in Scheme 3. Although C<sub>2</sub>H<sub>4</sub> coordination was reversible, such that removal of the ethylene atmosphere under vacuum restored the original black color of complex 3-Ir<sup>+</sup>, upon standing at room temperature under C<sub>2</sub>H<sub>4</sub> over a period of 24 h, adduct 5-Ir<sup>+</sup> rearranged irreversibly to the hydride complex 6-Ir<sup>+</sup>. As depicted in Scheme 3, coordination of the iridium(III) center of this species is completed by a chelating carbene–pyridine ligand resulting from C–N coupling between a molecule of C<sub>2</sub>H<sub>4</sub> and the amido nitrogen atom of the original pyridylamido ligand.

The adduct 5-Ir<sup>+</sup> could only be studied by solution NMR spectroscopy because of the facility of C<sub>2</sub>H<sub>4</sub> dissociation, whereas the stable complex 6-Ir<sup>+</sup> was isolated as a crystalline solid and fully characterized by microanalytical, spectroscopic (IR and NMR), and X-ray data. No <sup>1</sup>H NMR resonances were recorded at room temperature for the coordinated ethylene molecule of 5-Ir<sup>+</sup>, but at –40 °C, a characteristic AA'BB' multiplet was observed centered at 4.02 ppm, with δ<sub>A</sub> nearly equal to δ<sub>B</sub>. In the <sup>13</sup>C{<sup>1</sup>H} NMR spectrum registered also at –40 °C, the corresponding signal appeared at 61.7 ppm. A comparison with the δ value found for free C<sub>2</sub>H<sub>4</sub> of 123 ppm reveals a Δδ shift to low frequency of around 61 ppm. This shift is smaller than that recorded for the related [(η<sup>5</sup>-C<sub>5</sub>Me<sub>5</sub>)Rh(P<sup>^</sup>C)(C<sub>2</sub>H<sub>4</sub>)]<sup>+</sup> species of cyclometalated PPr<sub>2</sub>Xyl (ca. δ 47 and Δδ 76 ppm),<sup>18</sup>

Scheme 2. Synthesis of the Carbonyl Complexes 4-Ir<sup>+</sup> and 4-Rh<sup>+</sup>

<sup>a</sup>Reactions were performed at room temperature under 1 bar of CO.

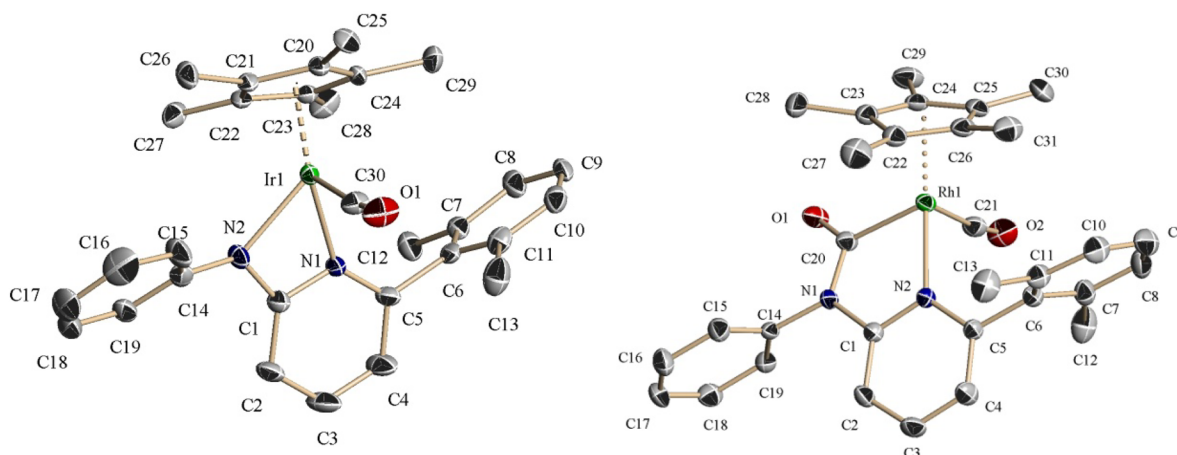
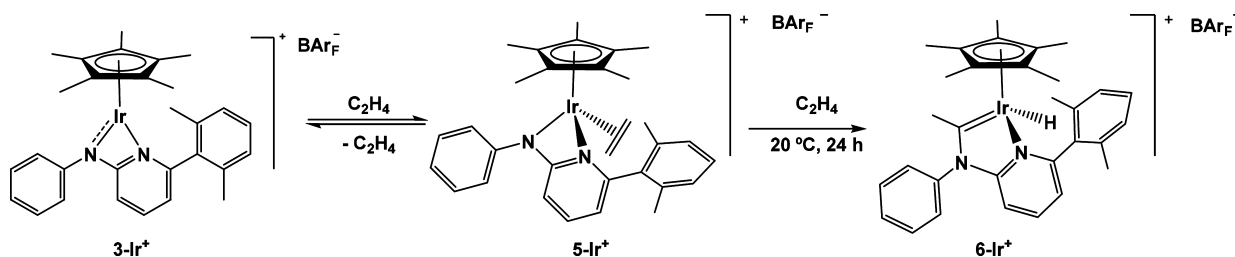


**Figure 3.** X-ray structure of complexes **4-Ir<sup>+</sup>** and **4-Rh<sup>+</sup>** (30% ellipsoids, anion  $\text{BARF}^-$ , and hydrogen atoms were omitted for clarity). Selected bond lengths (Å) and angles (deg) for **4-Ir<sup>+</sup>**: Ir1–N1 2.137(7), Ir1–C21 2.163(6), Ir1–N2 2.089(6), Ir1–C22 2.232(7), Ir1–C30 1.874(8), Ir1–C23 2.259(8), O1–C30 1.145(9), Ir1–C24 2.216(10), Ir1–C20 2.181(7); C30–Ir1–N1 94.2(3), C1–N1–Ir1 94.3(5), C30–Ir1–N2 94.5(3), C1–N2–Ir1 96.3(5), N2–Ir1–N1 62.0(2), N1–C1–N2 107.1(8). Selected bond lengths (Å) and angles (deg) for **4-Rh<sup>+</sup>**: Rh1–N2 2.152(3), Rh1–C21 1.908(5), O2–C21 1.115(6), Rh1–C20 2.026(4), O1–C20 1.200(5), Rh1–C22 2.235(5), Rh1–C23 2.251(5), Rh1–C24 2.157(4), Rh1–C25 2.262(4), Rh1–C26 2.333(5); C21–Rh1–N2 94.55(17), C21–Rh1–C20 88.9(2), C20–Rh1–N2 79.13(15), N1–C20–Rh1 111.9(3), C1–N2–Rh1 112.5(3), N2–C1–N1 115.0(4).

### Scheme 3. Reaction of Cation **3-Ir<sup>+</sup>** with Ethylene



suggesting reduced  $\pi$ -back-bonding to ethylene in the present complex.

The existence of hydride and carbene ligands in the formulation proposed for the isomeric complex **6-Ir<sup>+</sup>** is strongly backed by spectroscopic data. The Ir–H bond gives rise to an IR band at  $2096\text{ cm}^{-1}$  because of its stretching vibration and to a shielded  $^1\text{H}$  NMR resonance at  $-16.42\text{ ppm}$  that appears as a broad singlet. In turn, the  $^{13}\text{C}$  nucleus of the carbene ligand resonates at  $235.9\text{ ppm}$ . **Figure 4** shows the solid-state structure of the molecules of this complex, corroborating the formulation anticipated in **Scheme 3** on the basis of spectroscopic data. The Ir–C20 bond to the carbene carbon atom has a length of  $1.911(12)\text{ Å}$ , very similar to the distances found for other cationic and neutral carbene complexes of iridium(III) reported by our group.<sup>18–21</sup> The Ir1–N1 bond to the pyridine ring has a distance of  $2.113(8)\text{ Å}$ , which is also comparable to the Ir–N<sub>pyridine</sub> distances found in related complexes described in this paper or previously.<sup>1,2</sup>

By analogy with previously reported studies, the  $\alpha$ -H elimination that leads to complex **6-Ir<sup>+</sup>** is expected to be reversible.<sup>18–23</sup> Indeed, observation of the hydride resonance of **6-Ir<sup>+</sup>** as a broad singlet (vide supra) may be suggestive of fast equilibration of this complex with undetectable concentrations of the cyclic alkylpyridine solvent species **6-Ir<sup>+</sup>CD<sub>2</sub>Cl<sub>2</sub><sup>+</sup>** (**Scheme 4**), resulting from fast migratory insertion of the carbene ligand of **6-Ir<sup>+</sup>** into the Ir–H bond, promoted by coordination of  $\text{CD}_2\text{Cl}_2$ .<sup>19a</sup> Reaction of **6-Ir<sup>+</sup>** with an excess of  $\text{PMe}_3$  triggered the anticipated 1,2-H shift from iridium to the carbene carbon atom, although

subsequent chemical changes must be invoked to account for the chemical constitution of the resulting product **7-Ir<sup>+</sup>**. As specified in **Scheme 4**, this complex incorporates two molecules of  $\text{PMe}_3$  and in addition contains a  $\beta$ -functionalized linear alkyl Ir– $\text{CH}_2\text{CH}_2\text{N}_{\text{amido}}(\text{Ph})^-$ , which is formally derived from a direct N–C coupling reaction between the amido terminus of the Ap ligand and a molecule of  $\text{C}_2\text{H}_4$ . In other words, beyond accomplishing migratory insertion reactivity between the hydride and carbene units of **6-Ir<sup>+</sup>**,  $\text{PMe}_3$  induces a branched-to-linear isomerization of the resulting secondary alkyl ligand,  $\text{IrCH}(\text{Me})\text{N}(\text{Ph})^-$ , and decoordination of its pyridine end. As discussed in the following paragraphs dealing with computational studies, the reactivity represented in **Schemes 3** and **4** entails competitive  $\alpha$ - and  $\beta$ -H elimination reactions and their microscopic reverse migratory insertions of carbene and olefin functionalities into Ir–H bonds. Monitoring of the reaction between **6-Ir<sup>+</sup>** and  $\text{PMe}_3$  by  $^{31}\text{P}\{^1\text{H}\}$  NMR spectroscopy at low temperature (from  $-80$  to  $+20\text{ °C}$ ) did not provide additional useful information. The immediate formation of a complex mixture of products occurred at low temperatures, and at  $0\text{ °C}$ , this mixture slowly converted into the final complex **7-Ir<sup>+</sup>**, which became the only observable species after 15 h at room temperature.

Although the NMR properties of **7-Ir<sup>+</sup>** permitted unambiguous structural identification, additional support was sought through X-ray crystallography. The  $^{31}\text{P}\{^1\text{H}\}$  NMR spectrum contains the expected singlet with a chemical shift of  $-45.4\text{ ppm}$ . In the  $^1\text{H}$  NMR spectrum, the two equivalent  $\alpha$ -alkyl protons,  $\text{IrCH}_2\text{CH}_2^-$ , appear as a multiplet centered at  $1.47\text{ ppm}$ , as a

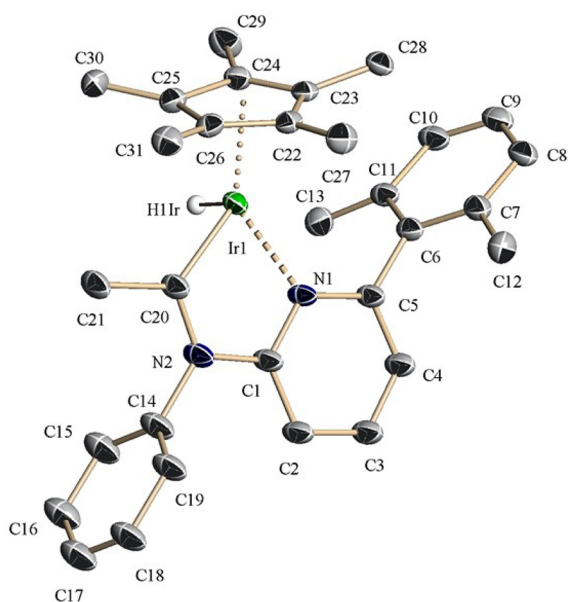


**Figure 4.** X-ray structure of complex **6-Ir<sup>+</sup>** (30% ellipsoids, hydrogen atoms, and anion  $\text{BAr}_F^-$  were omitted for clarity). Selected bond lengths (Å) and angles (deg): Ir1–C20 1.911(12), Ir1–C23 2.340(11), Ir1–N1 2.113(8), Ir1–C24 2.280(13), Ir1–H(1Ir) 1.6070, Ir1–C25 2.161(12), N2–C20 1.345(14), Ir1–C26 2.226(10), Ir1–C22 2.284(11); C20–Ir1–N1 78.4(4), C20–N2–C1 115.5(10), C20–Ir1–H(1Ir) 89.1, N1–C1–N2 116.2(10), N1–Ir1–H(1Ir) 87.0, N2–C20–Ir1 118.8(8), C1–N1–Ir1 111.1(7).

consequence of coupling to the two  $\beta$ -hydrogen atoms and the two  $^{31}\text{P}$  nuclei. Likewise, the  $\text{IrCH}_2\text{CH}_2-$  resonance is a multiplet, albeit substantially deshielded (3.67 ppm). Corresponding  $^{13}\text{C}\{^1\text{H}\}$  resonances appear at  $-7.1$  and  $+56.0$  ppm, with two- and three-bond coupling to the  $^{31}\text{P}$  nuclei of 7 and 5 Hz, respectively.

**Figure 5** presents an ORTEP perspective view of the molecular structure of complex **7-Ir<sup>+</sup>**. As for related complexes, coordination of the  $\text{C}_5\text{Me}_5$  ring is fairly symmetrical, with Ir–C distances spanning the rather narrow range 2.236(5)–2.281(4) Å. The two Ir–P bonds have similar distances and are indistinguishable within experimental error [2.2734(12) and 2.2854(13) Å], and the  $\sigma$  Ir–C bond to C21 has a length of 2.140(4) Å.

Similar to the iridium cation **3-Ir<sup>+</sup>**, the rhodium analogue **3-Rh<sup>+</sup>** reacted instantly with ethylene. Rather disappointingly, as discussed below, a very complex mixture of compounds was observed even at low temperature ( $-80$  °C), considerably limiting the synthetic and mechanistic utility of this reaction. Nevertheless, some useful information could be collected and will be briefly discussed. Mixing the rhodium complex **3-Rh<sup>+</sup>** and  $\text{C}_2\text{H}_4$  at  $0$  °C caused immediate consumption of the metal reagent and generation of a complex manifold of products.

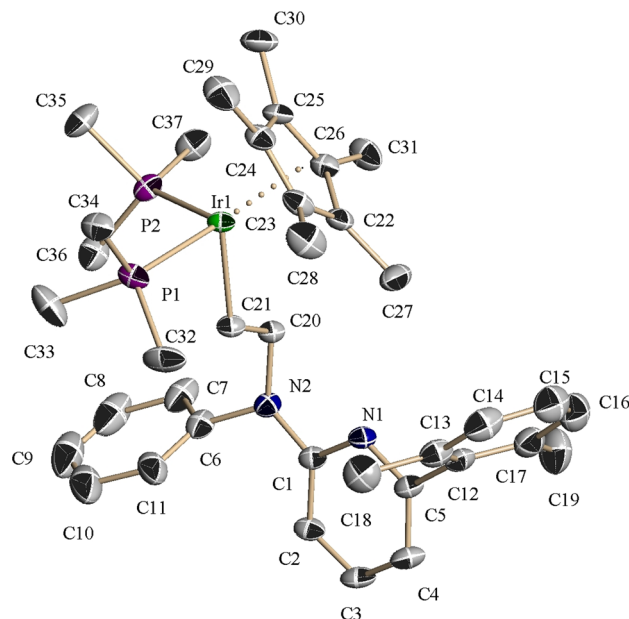
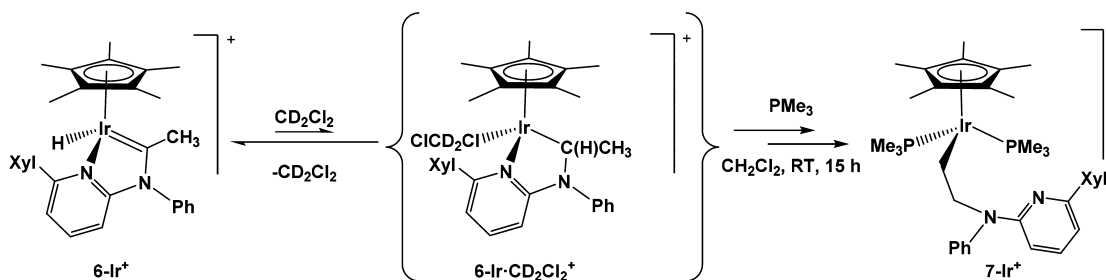


**Figure 5.** X-ray structure of complex **7-Ir<sup>+</sup>** (30% ellipsoids, hydrogen atoms, and anion  $\text{BAr}_F^-$  were omitted for clarity). Selected bond lengths (Å) and angles (deg): Ir1–C21 2.140(4), Ir1–C23 2.246(5), Ir1–P1 2.2854(13), Ir1–C24 2.278(4), Ir1–P2 2.2734(12), Ir1–C25 2.281(4), C20–C21 1.534(6), Ir1–C26 2.236(5), Ir1–C22 2.267(5); P1–Ir1–P2 96.22(5), Ir1–C21–C20 117.6(3), P1–Ir1–C21 83.23(13), C21–C20–N2 112.0(4), C21–Ir1–P2 89.86(13).

The  $^1\text{H}$  NMR spectrum of this mixture (**Figure S23**) contained discernible  $\eta^5\text{-C}_5\text{Me}_5$  resonances between 1.2 and 1.6 ppm for at least four rhodium compounds. One of these species originated, in addition, a significantly shielded doublet resonance at  $-0.21$  ppm ( $^3J_{\text{HH}} \sim 6$  Hz). Keeping in mind the results already described for the analogous iridium system and by similarity with NMR data reported in the literature for the  $\text{Rh}\cdots\text{CH}_3$   $\delta$ -agostic bond found in the cationic rhodium(III)  $[(\eta^5\text{-C}_5\text{Me}_5)\text{Rh}(\text{H})(\text{PMeXyl}_2)]^+$  complex ( $-0.02$  ppm),<sup>24</sup> it can be proposed that one of the components of the said mixture contains a chelating secondary alkylpyridine ligand in which the  $\text{RhC}(\text{H})\text{MeCH}_2\text{N}$ -unit is further engaged in a  $\beta$ -agostic methyl interaction (structure **5-Rh<sup>+</sup>** in **Figure 6**). In one of the many crystallization attempts effected, a few single crystals were obtained, and while no full NMR characterization of the pure isolated complex could be accomplished, its molecular structure was disclosed by a single-crystal XRD study. The ORTEP view of the molecules of **5-Rh<sup>+</sup>** is shown on the right-hand-side of **Figure 6** and provides unequivocal proof for a C–N coupling reaction alike that described for the analogous iridium complex. As can be seen, the complex contained a five-membered  $\text{C}^*\text{N}$  metallacycle

#### Scheme 4. Reaction of Complex **6-Ir<sup>+</sup>** with $\text{PMe}_3$



E

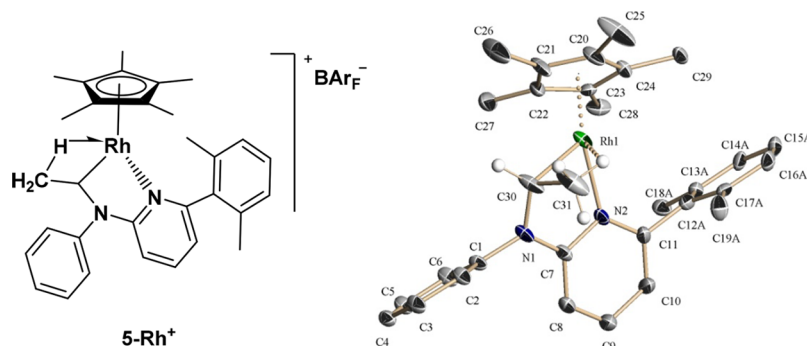
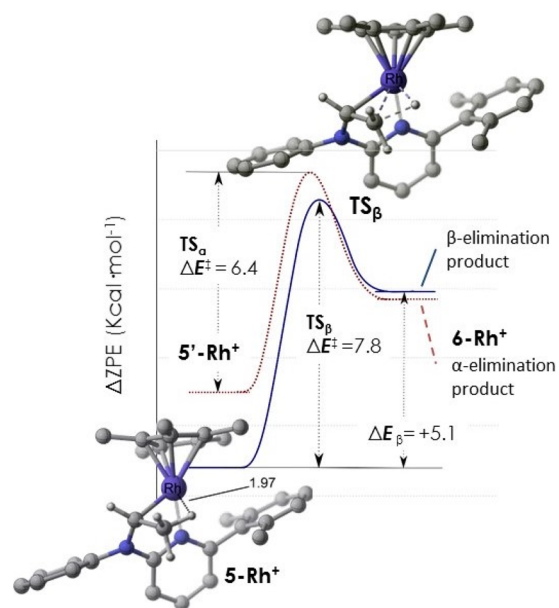


**Figure 6.** X-ray structure of complex  $5\text{-Rh}^+$  (30% ellipsoids, hydrogen atoms, and anion  $\text{BAR}_F^-$  were omitted for clarity). Selected bond lengths ( $\text{\AA}$ ) and angles (deg):  $\text{Rh1-C30}$  2.009(7),  $\text{Rh1-C31}$  2.362(7),  $\text{Rh1-C21}$  2.153(9),  $\text{Rh1-H(C31)}$  1.9373,  $\text{Rh1-C22}$  2.123(8),  $\text{Rh1-N2}$  2.153(5),  $\text{Rh1-C23}$  2.179(6),  $\text{N1-C30}$  1.431(8),  $\text{Rh1-C24}$  2.259(6),  $\text{Rh1-C20}$  2.188(7);  $\text{C30-Rh1-N2}$  78.2(3),  $\text{C7-N1-C30}$  118.3(5),  $\text{C30-Rh1-H(C31)}$  63.9,  $\text{N1-C7-N2}$  114.5(5),  $\text{N2-Rh1-H31C}$  88.5,  $\text{N1-C30-Rh1}$  111.5(4),  $\text{C7-N2-Rh1}$  112.3(4),  $\text{C31-H31C-Rh1}$  103.15.

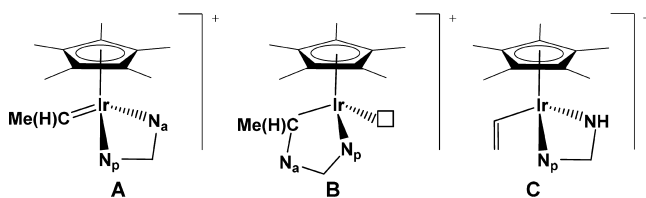
consisting of secondary alkyl and pyridine ligands, with the rhodium(III) center being additionally decorated by a  $\beta$ -agostic interaction, helping to achieve an 18-electron count. Despite the uncertainties in determining the positions of the hydrogen atoms by XRD, the metric parameters for the  $\text{RhCH}(\text{CH}_3)$ – linkage are in agreement with the existence in the solid state of a  $\text{Rh}\cdots\text{CH}_3$   $\beta$ -agostic interaction. The  $\text{Rh1-C31}$  distance is relatively short at 2.362(7)  $\text{\AA}$ , and both the  $\text{Rh1-H(C31)}$  distance of 1.937  $\text{\AA}$  and the  $\text{Rh1-H-C31}$  angle of  $103.15^\circ$  are well in the 1.8–2.3  $\text{\AA}$  and  $90$ – $140^\circ$  ranges commonly found, for such bonds.<sup>25</sup> Although the limited experimental evidence obtained for the reaction of  $3\text{-Rh}^+$  and  $\text{C}_2\text{H}_4$  prevents a proper discussion of these results, it should be noted that observation of the agostic structure for  $5\text{-Rh}^+$  is in line with common knowledge that agostic bonds are favored for cationic complexes of first- and second-row metals, whereas their third-row counterparts prefer the isomeric hydride formulation.<sup>25,26</sup> Computational data discussed next are also in accordance with these observations.

The structure presented in Figure 6 for complex  $5\text{-Rh}^+$  may be viewed as a model for the intermediate preceding  $\beta$ -H elimination to furnish an isomeric hydride–alkene product. DFT calculations revealed that while an energy barrier of only 7.8 kcal mol<sup>−1</sup> needs to be overcome (Figure 7), the  $\beta$ -H elimination reaction is thermodynamically uphill by 5.1 kcal mol<sup>−1</sup>. Moreover, in a different conformation,  $5'\text{-Rh}^+$ , which is just 2.2 kcal mol<sup>−1</sup> above the observed structure (Figure 7),  $\alpha$ -H elimination to yield a hydride–alkylidene complex analogous to  $6\text{-Ir}^+$ , thereby containing an N-stabilized carbene ligand, could occur with an affordable energy barrier of 6.4 kcal mol<sup>−1</sup>. Notwithstanding, the purported hydride–carbene rhodium complex would be thermodynamically unstable in comparison with the isolated complex  $5\text{-Rh}^+$  and also with the conformation  $5'\text{-Rh}^+$ .

**Computational Studies on the Reaction of  $3\text{-Ir}^+$  with  $\text{C}_2\text{H}_4$ .** The nature of the carbene ligand of product  $6\text{-Ir}^+$ , which besides the N-heteroatom features a methyl substituent at the carbene carbon, denotes that  $6\text{-Ir}^+$  forms by  $\alpha$ -H elimination from a chelating pyridine–alkyl ligand like intermediate  $6\text{-Ir}\cdot\text{ClCD}_2\text{Cl}^+$  of Scheme 4 (vide supra). Hence, we initially envisioned a reaction route implicating a highly reactive cationic iridium ethylidene group,  $[\text{Ir}]=\text{C}(\text{H})\text{Me}$ , with a structure akin to **A** in Figure 8, formally arising from an iridium-promoted tautomerization of coordinated  $\text{C}_2\text{H}_4$  in  $5\text{-Ir}^+$ . The said prototropism could be followed by ethylidene migratory insertion into the  $\text{Ir-N}_{\text{amido}}$  bond, yielding an unsaturated branched alkyl (**B** in Figure 8), which would convert into the product by  $\alpha$ -H elimination.

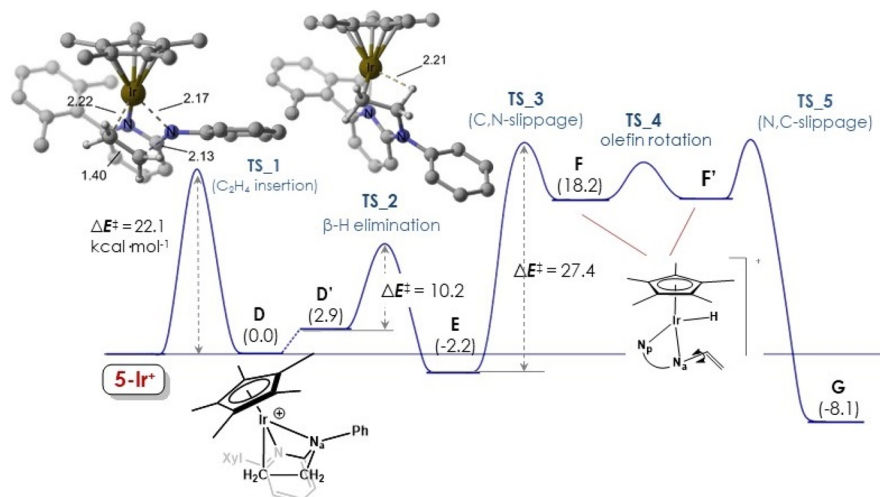
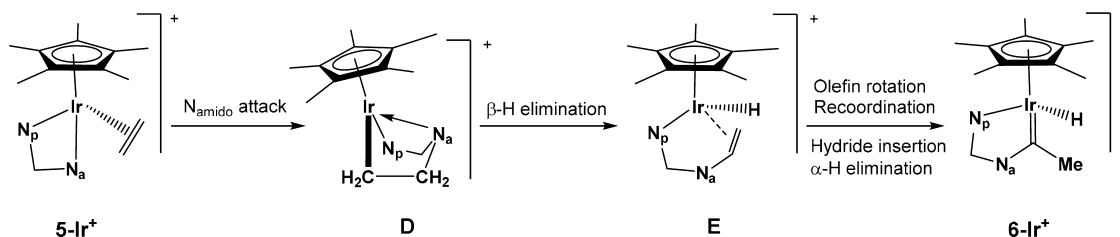


**Figure 7.** Calculated energy profiles for  $\beta$ -H (solid line) and  $\alpha$ -H (dotted line) elimination from the appropriate conformer of  $5\text{-Rh}^+$ . Optimized geometries of  $5\text{-Rh}^+$  and the transition state for  $\beta$ -H elimination. Zero-point-corrected potential energies calculated in dichloromethane relative to the ethylene adduct.



**Figure 8.** Possible intermediates for an ethylidene route to complex  $6\text{-Ir}^+$ .

A direct 1,2-shift within the coordinated ethylene molecule could account for the ethylene-to-ethylidene tautomerism, similar to well-established metal-promoted acetylene-to-vinylidene rearrangements.<sup>27</sup> While the  $\text{C}_2\text{H}_4$  and  $\text{C}_2\text{H}_2$  tautomerizations are strongly endothermic (ca. 80 and 45 kcal mol<sup>−1</sup> for the former<sup>21a</sup> and latter,<sup>27</sup> respectively), the relative energies of the corresponding  $\pi$ -hydrocarbon and carbene isomers change dramatically in the coordination sphere of transition metals. In many reported examples, the driving force for the isomerization is largely associated with the strong electronic interaction

Scheme 5. Key Intermediates in the Proposed Migratory Insertion Leading to Complex 6-Ir<sup>+</sup>

**Figure 9.** Energy profile including the initial steps of the migratory insertion path. Zero-point-corrected potential energies calculated in dichloromethane relative to the ethylene adduct.

between the metal and carbene-type ligand.<sup>21a,27c</sup> Indeed, our computational studies evince that the ethylidene intermediate **A** (Figures 8 and S45 and S46) is only 12.5 kcal mol<sup>-1</sup> less stable than its olefin isomer **5-Ir<sup>+</sup>** and, moreover, that the consequent N–C bond formation resulting from a nucleophilic attack of the Ir–N<sub>amido</sub> bond to the Ir=C(H)Me one needs to overcome a barrier of just 12.1 kcal mol<sup>-1</sup>. Nevertheless, all attempts to model the direct 1,2-H shift within the Ir–C<sub>2</sub>H<sub>4</sub> linkage of **5-Ir<sup>+</sup>** gave unrealistically high energy barriers, which justified ruling out this path.

As a variant to the direct 1,2-H shift, we analyzed a shuttling function<sup>28–30</sup> of the Ir–N<sub>amido</sub> unit, abstracting first an olefinic hydrogen atom to yield an iridium vinyl **C** (Figures 8 and S46) and then protonating the  $\beta$ -carbon atom of the ligated vinyl to produce **A**. Once again, whereas structure **C** is energetically feasible, lying in energy 10.5 kcal mol<sup>-1</sup> above **5-Ir<sup>+</sup>**, conversion of the latter into the former requires one to surmount a barrier of ca. 32.6 kcal mol<sup>-1</sup>, which is at odds with the experimental conditions. Aside from that, this barrier is significantly higher than the topmost step in the migratory insertion mechanism discussed next.

**Scheme 5** summarizes the mechanistic route that implies migratory insertion of ethylene into the Ir–N<sub>amido</sub> bond of complex **5-Ir<sup>+</sup>**. Figures 9 and 10 display relevant information on key steps of the calculated energy profile. The migratory insertion is relatively facile, and an energy barrier of  $\Delta E^\ddagger = 22.1$  kcal mol<sup>-1</sup> needs be surpassed to afford intermediate **D** (**Scheme 5** and **Figure 9**), which is in actuality isoenergetic with the initial (pyridylamido)ethylene complex **5-Ir<sup>+</sup>**. The proposed intermediate exhibits a six-membered chelating moiety consisting of pyridine and alkyl ends and becomes stabilized by the formation of a dative covalent bond between iridium and the

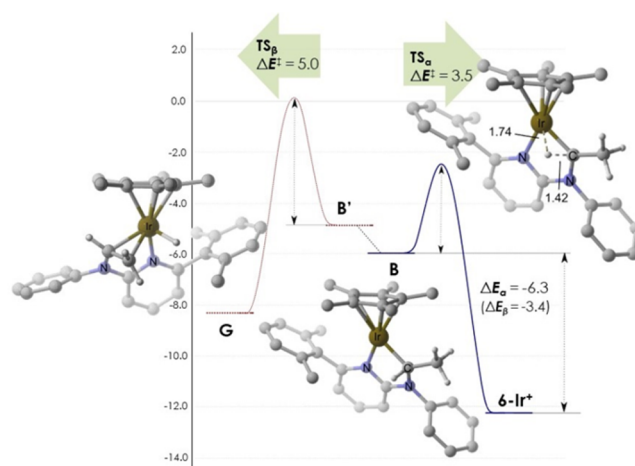


**Figure 10.** DFT-calculated energy profiles for  $\alpha$ -H (solid line) and  $\beta$ -H (dotted line) elimination from the appropriate conformer, **B** or **B'**, and optimized geometries of relevant species. Zero-point-corrected potential energies calculated in dichloromethane relative to **5-Ir<sup>+</sup>**.

former N<sub>amido</sub> function, now converted into an NH amino one (Ir–N<sub>amino</sub> distance of 2.27 Å vs 2.15 Å for Ir–N<sub>pyridine</sub>).

Elongation of the Ir–N<sub>amino</sub> distance of **D** to 3.00 Å results in a conformation, **D'** (Figures 9 and S47;  $\Delta E^\circ = 2.9$  kcal mol<sup>-1</sup>), from which  $\beta$ -H elimination can take place easily ( $\Delta E^\ddagger = 10.3$  kcal mol<sup>-1</sup>). As was already anticipated, the formation of **6-Ir<sup>+</sup>** from the resulting species **E** (**Figure 9**;  $\Delta E^\circ = -2.2$  kcal mol<sup>-1</sup>) requires a change of the coordinated face of the prochiral olefin. If this process is assisted by the amido nitrogen functionality, the barrier for Ir–C to Ir–N slippage required to allow olefin

dissociation to yield **F** (Figure 9) turned out to be rate-limiting ( $\Delta E^\ddagger = 27.4 \text{ kcal mol}^{-1}$  from **E**), but it is still more accessible than the hydrogen abstraction from  $\text{C}_2\text{H}_4$  discussed previously. As expected, rotation of the  $\text{N}_a\text{-CH=CH}_2$  bond and recoordination of the olefin through the other face to give the hydride-olefin species **G**, i.e., stereoisomer of **E**, are fast, and the latter step is also very exothermic ( $\Delta E^\circ = -26.3 \text{ kcal mol}^{-1}$  from **F**). From this point, formation of  $6\text{-Ir}^+$  requires hydride insertion and  $\alpha$ -elimination from **B**, both steps having accessible energy barriers. Notice that  $\alpha$ -H elimination from **B** appears faster than  $\beta$ -H elimination from **B'** and, more significantly, that the energy return from the former process to produce the carbene product  $6\text{-Ir}^+$  is larger than that associated with  $\beta$ -H elimination from **B'** to generate the unobserved hydride-olefin tautomer **G**. It is worth recalling that although  $\beta$ -H elimination is usually faster than  $\alpha$ -H elimination when the two reactions can compete, examples are known where the opposite is true. Specifically, in sterically congested systems in which the  $\text{M-C}_\alpha\text{-C}_\beta\text{-H}$  atoms cannot readily adopt the required syn approximately coplanar arrangement,<sup>31</sup> the formation of  $\alpha$ -agostic bonds and  $\alpha$ -H elimination may become faster than the corresponding processes for  $\beta$ -hydrogen atoms.<sup>21,23,32</sup>

**Reactions of Iridium and Rhodium Complexes  $3\text{-M}^+$  with  $\text{H}_2$ .** The title reactions proceeded much as expected on the basis of previous studies.<sup>1,2</sup> Briefly, we recall that catalytic amounts of  $\text{H}_2$  promote reversible isomerization of the

aminopyridinate ligand between classical  $\kappa^2\text{-N,N}$ -bidentate binding and an unprecedented  $\kappa\text{-N},\eta^3$ -pseudoallyl coordination, as depicted in Scheme 6 (left part) for  $3\text{-Ir}^+$  and  $8\text{-Ir}^+$ . The isomerization implies reversible formation and cleavage of H-H, C-H, and N-H bonds. Experimental and computational studies<sup>1,2</sup> support the mechanistic pathway presented in Scheme S2.

The treatment of  $3\text{-Ir}^+$  with an excess of  $\text{H}_2$  yielded the known binuclear hydride  $\{[(\eta^5\text{-C}_5\text{Me}_5)\text{Ir}]_2(\mu\text{-H})_3\}^+$ ,<sup>33</sup> whereas catalytic amounts of  $\text{H}_2$  (ca. 2 mol %) promoted isomerization of the Ap ligand of  $3\text{-Ir}^+$  to the  $\eta^3$ -benzylic-pyridine coordination found in the new complex  $8\text{-Ir}^+$  (Scheme 6). The prototropic rearrangement resulted in a  $3\text{-Ir}^+ \rightleftharpoons 8\text{-Ir}^+$  equilibrium mixture of ca. 1:3, with a half-life,  $t_{1/2}$ , of about 1.2 h ( $20^\circ\text{C}$ ,  $\text{CD}_2\text{Cl}_2$ ). Under similar experimental conditions and a  $\text{H}_2$  concentration of 1.6 mol %, the analogous complex in which the amido nitrogen aryl substituent was  $2,6\text{-Pr}_2\text{C}_6\text{H}_3$  instead of  $\text{C}_6\text{H}_5$  equilibrated with  $t_{1/2} = 9.1$  h. This difference in the rate of almost 1 order of magnitude clearly reflects the importance of the steric effects of the amido nitrogen aryl substituent in the reactivity of complexes like  $3\text{-M}^+$ .

Spectroscopic data for  $8\text{-Ir}^+$  are similar to those recorded for related complexes.<sup>1</sup> The NH resonance is, however, slightly deshielded relative to the values found for analogous complexes (6.25 vs ca. 5.94 ppm).<sup>1</sup> It is tempting to associate this shift with the relatively short  $\text{Ir}\cdots\text{HN}$  contact of 2.89 Å observed in the solid-state molecular structure of the complex (Figure 11, left).

**Scheme 6.**  $\text{H}_2$ -Catalyzed Isomerization of the Aminopyridinate Ligand of  $3\text{-Ir}^+$  and Formation of the Carbonyl Complex  $9\text{-Ir}^+$

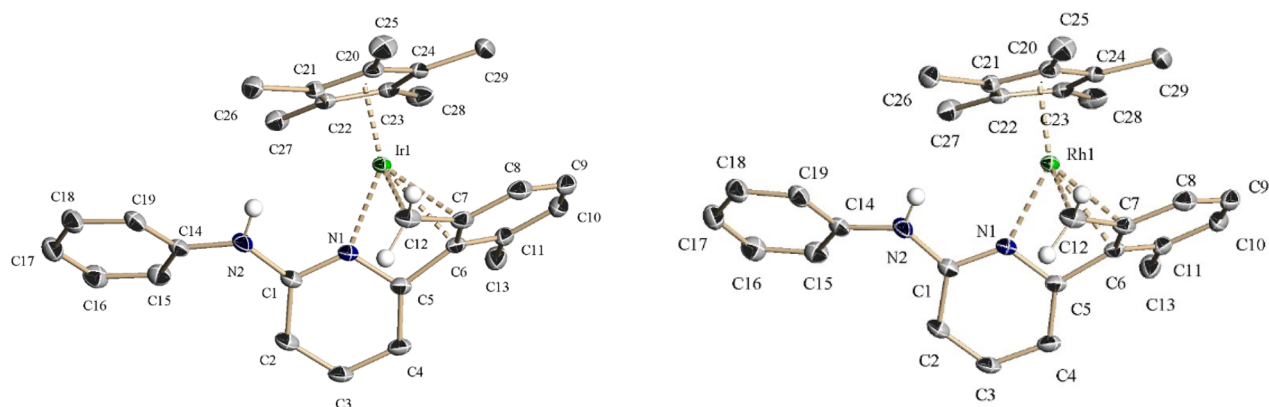
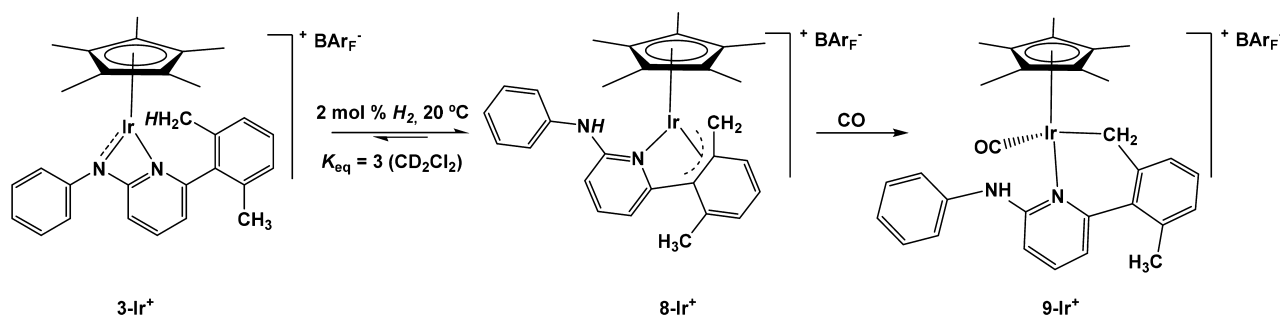


**Figure 11.** X-ray structures of complexes  $8\text{-Ir}^+$  (left) and  $8\text{-Rh}^+$  (right) (30% ellipsoids, hydrogen atoms, and anion  $\text{BAR}_F^-$  were omitted for clarity). Selected bond lengths (Å) and angles (deg) for  $[8\text{-Ir}]\text{BAR}_F^-$ : Ir1–N1 2.086(3), C10–C11 1.378(6), Ir1–C6 2.387(4), C6–C11 1.423(6), Ir1–C7 2.252(4), Ir1–C20 2.170(3), Ir1–C12 2.118(4), Ir1–C21 2.153(4), C6–C7 1.449(5), Ir1–C22 2.202(3), C7–C12 1.449(6), Ir1–C23 2.225(4), C7–C8 1.423(6), Ir1–C24 2.187(4), C8–C9 1.355(7), Ir1–H(N2) 2.891, C9–C10 1.408(6); N1–Ir1–C6 62.04(12), N1–Ir1–C12 80.11(14), C7–Ir1–C6 36.27(13), N1–C5–C6 108.5(3), C12–Ir1–C7 38.59(16), N1–C1–N2 115.1(3). Selected bond lengths (Å) and angles (deg) for  $[8\text{-Rh}]\text{BAR}_F^-$ : Rh1–N1 2.101(3), C10–C11 1.372(7), Rh1–C6 2.379(4), C6–C11 1.428(7), Rh1–C7 2.237(4), Rh1–C20 2.176(4), Rh1–C12 2.124(5), Rh1–C21 2.155(4), C6–C7 1.441(6), Rh1–C22 2.191(4), C7–C12 1.437(7), Rh1–C23 2.218(4), C7–C8 1.432(7), Rh1–C24 2.174(4), C8–C9 1.350(8), Rh1–H(N2) 2.987, C9–C10 1.406(8); N1–Rh1–C6 62.43(14), N1–Rh1–C12 81.00(17), C7–Rh1–C6 36.21(16), N1–C5–C6 110.3(4), C12–Rh1–C7 38.37(19), N1–C1–N2 115.4(4).

Nonetheless, recalling that hydrogen positions determined by X-ray studies are not particularly accurate and that the Ir...HN contact in **8-Ir<sup>+</sup>** is longer than the known Ir...HC agostic bonds,<sup>34</sup> such a NH...Ir interaction must be very weak and most probably meaningless in terms of electron density sharing. A close similarity of **8-Ir<sup>+</sup>** to earlier analogues was also found in the reaction with CO (Scheme 6) that occurred with a  $\eta^3$ -to- $\eta^1$ -benzyl coordination change and formation of the carbonyl complex **9-Ir<sup>+</sup>**. The latter exhibits  $\bar{\nu}(\text{CO})$  at 2029 cm<sup>-1</sup> (see the Experimental Section).

Monitoring the progress of the reaction of **3-Ir<sup>+</sup>** with an excess of H<sub>2</sub> (1 bar) allowed observation of a hydride intermediate in high spectroscopic yield (−6.32 ppm, relative intensity 1 H). Isolation of this complex proved unattainable because in the presence of H<sub>2</sub> it converted quickly to  $\{[(\eta^5\text{-C}_5\text{Me}_5)\text{Ir}]_2(\mu\text{-H})_3\}^+$ , whereas in the absence of this gas, it yielded, also rapidly, the 1:3 equilibrium mixture of **3-Ir<sup>+</sup>** and **8-Ir<sup>+</sup>**. No NH resonance or other relevant NMR data could, however, be assigned with certainty to this intermediate, which keeps us from putting forward a definitive structural proposal.

Complex **3-Rh<sup>+</sup>** also reacted quickly with 1 bar of H<sub>2</sub> at room temperature although a complex mixture of compounds was obtained including  $\{[(\eta^5\text{-C}_5\text{Me}_5)\text{Rh}]_2(\mu\text{-Cl})_3\}^+$ .<sup>35</sup> At least two  $\eta^4\text{-C}_5\text{Me}_5\text{H}$ -containing complexes<sup>36</sup> were detected by NMR, the latter possibly related to those that were fully characterized for bulkier aminopyridinate ligands.<sup>2</sup> Likewise, the  $\eta^3$ -benzyl complex **8-Rh<sup>+</sup>** resulting from the H<sub>2</sub>-catalyzed isomerization of the aminopyridinate ligand was detected in the crude reaction mixture. The latter complex was subsequently generated in moderate quantities (ca. 50% spectroscopic yield) using substoichiometric amounts of H<sub>2</sub> (60 mol %). Complex **8-Rh<sup>+</sup>** was fully characterized. Its X-ray molecular structure is presented in Figure 11 (right-hand side) and features metrical parameters for the metal- $\eta^3$ -benzyl moiety similar to those of analogous complexes.

## CONCLUSIONS

This work demonstrated that the M–N<sub>amido</sub> bond of the pyridylamido complexes  $[(\eta^5\text{-C}_5\text{Me}_5)\text{M}(\text{N}^{\wedge}\text{N})]^+$  (**3-M<sup>+</sup>**) readily activates CO, C<sub>2</sub>H<sub>4</sub>, and H<sub>2</sub>. Whereas CO and C<sub>2</sub>H<sub>4</sub> brought about migratory insertion reactivity, H<sub>2</sub> catalyzed a prototropic rearrangement within the Ap ligand, whereby remote transfer of a benzylic hydrogen atom from the pyridine xylyl substituent to the amido nitrogen atom occurred readily in a reversible fashion.

Only **3-Rh<sup>+</sup>** experienced CO migratory insertion into the Rh–N<sub>amido</sub> bond, expanding the original four-membered Rh–N–C–N ring to a five-membered pyridine–carbamoyl rhodacycle, whereas for iridium, the stronger M–N<sub>amido</sub> bond decisively retarded the migratory CO insertion step, affording the carbonyl adduct **4-Ir<sup>+</sup>** as the only observable product. In contrast, **3-Ir<sup>+</sup>** formed easily, albeit reversibly, the ethylene adduct **5-Ir<sup>+</sup>**, which rearranged spontaneously by migratory insertion, with the end product of the reaction being the hydride N-substituted alkylidene complex **6-Ir<sup>+</sup>**. DFT studies reinforced a mechanistic scheme encompassing irreversible C–N bond formation followed by reversible  $\beta$ - and  $\alpha$ -H elimination reactions.

## EXPERIMENTAL SECTION

**General Procedures.** Microanalyses were performed by the Microanalytical Service of the Instituto de Investigaciones Químicas (Sevilla, Spain). IR spectra were obtained from a Bruker Vector 22 spectrometer. The mass spectrometry (MS) spectra were obtained at the Mass Spectroscopy Service of the University of Sevilla. The NMR instruments were Bruker DRX-500, DRX-400, and DPX-300

spectrometers. Spectra were referenced to external SiMe<sub>4</sub> ( $\delta$  0 ppm) using the residual protio solvent peaks as internal standards (<sup>1</sup>H NMR experiments) or the characteristic resonances of the solvent nuclei (<sup>13</sup>C NMR experiments). Spectral assignments were made by routine one- and two-dimensional NMR experiments where appropriate. All manipulations were performed under dry, oxygen-free dinitrogen, following conventional Schlenk techniques. The crystal structures were determined in a Bruker-Nonius X8 Kappa diffractometer. Metal complexes  $[\text{Cp}^*\text{IrCl}_2]_2$ ,<sup>37</sup>  $[\text{Cp}^*\text{RhCl}_2]_2$ ,<sup>37</sup> and NaBAR<sub>F</sub><sup>38</sup> were prepared as previously described. The lithium salt of the aminopyridinate ligand employed in this work was prepared according to published procedures.<sup>1b</sup> The <sup>1</sup>H and <sup>13</sup>C{<sup>1</sup>H} NMR spectral data for the BAR<sub>F</sub> anion (BAR<sub>F</sub> = B[3,5-(CF<sub>3</sub>)<sub>2</sub>C<sub>6</sub>H<sub>3,4</sub>]) in CD<sub>2</sub>Cl<sub>2</sub> are identical for all complexes and therefore are not repeated below. <sup>1</sup>H NMR:  $\delta$  7.75 (s, 8 H, *o*-Ar), 7.58 (s, 4 H, *p*-Ar). <sup>13</sup>C{<sup>1</sup>H} NMR:  $\delta$  162.1 (q, <sup>1</sup>J<sub>CB</sub> = 37 Hz, *ipso*-Ar), 135.3 (*o*-Ar), 129.2 (q, <sup>2</sup>J<sub>CF</sub> = 31 Hz, *m*-Ar), 124.9 (q, <sup>1</sup>J<sub>CF</sub> = 273 Hz, CF<sub>3</sub>), 117.8 (*p*-Ar).

**Compound 2-Ir.** A toluene solution of LiAp (1 g, 3.57 mmol, 35 mL) at −50 °C was added to a suspension of  $[\text{Cp}^*\text{IrCl}_2]_2$  (1.4 g, 1.78 mmol) in toluene at −50 °C. The resulting mixture was stirred while allowing it to warm to room temperature and stirred further for a period of 14 h. The solution was filtered through Celite and the solvent removed under reduced pressure. <sup>1</sup>H NMR analysis of the crude reaction mixture showed only the presence of **2-Ir**, which was crystallized from CH<sub>2</sub>Cl<sub>2</sub>/hexane mixtures at −23 °C. Yield: 1.55 g (68%). <sup>1</sup>H NMR (C<sub>6</sub>D<sub>6</sub>, 25 °C):  $\delta$  7.54, 7.26, 6.96 (d, t, t, 2:2:1, <sup>3</sup>J<sub>HH</sub> ~ 7.5 Hz, 5 CH<sub>Ph</sub>), 7.06, 7.00, 6.96 (t, br d, br d, 1 H each, <sup>3</sup>J<sub>HH</sub> ~ 7.5 Hz, 3 CH<sub>Xyl</sub>), 6.80 (t, 1 H, <sup>3</sup>J<sub>HH</sub> = 7.9 Hz, 1 CH<sub>Pyr</sub>), 6.35 (d, 1 H, <sup>3</sup>J<sub>HH</sub> = 8.7 Hz, 1 CH<sub>Pyr</sub>), 5.81 (d, 1 H, <sup>3</sup>J<sub>HH</sub> = 7.0 Hz, 1 CH<sub>Pyr</sub>), 2.66, 2.13 (s, 3 H each, 2 Me<sub>Xyl</sub>), 1.16 (s, 15 H, 5 Me<sub>Cp\*</sub>). <sup>13</sup>C{<sup>1</sup>H} NMR (C<sub>6</sub>D<sub>6</sub>, 25 °C):  $\delta$  171.2, 156.4 (C<sub>q-Pyr</sub>), 146.3 (C<sub>q-Ph</sub>), 140.0, 139.0, 136.7 (C<sub>q-Xyl</sub>), 137.3, 108.9, 106.5 (CH<sub>Pyr</sub>), 129.0, 124.1, 122.1 (2:2:1, CH<sub>Ph</sub>), 128.5, 128.3, 127.0 (CH<sub>Xyl</sub>), 84.0 (C<sub>q-Cp\*</sub>), 21.9, 20.8 (Me<sub>Xyl</sub>), 9.1 (Me<sub>Cp\*</sub>). Elem anal. Calcd for C<sub>29</sub>H<sub>32</sub>ClIrN<sub>2</sub>: C, 54.7; H, 5.1; N, 4.4. Found: C, 54.6; H, 5.1; N, 4.5.

**Compound 2-Rh.** Following the procedure described above for **2-Ir** but using  $[\text{Cp}^*\text{RhCl}_2]_2$ , compound **2-Rh** was obtained in quantitative spectroscopic yield and was crystallized from CH<sub>2</sub>Cl<sub>2</sub>–hexane mixtures at −23 °C. Yield: 0.8 g (64%). <sup>1</sup>H NMR (C<sub>6</sub>D<sub>6</sub>, 25 °C):  $\delta$  7.65, 7.28 (d, t, 1:1, <sup>3</sup>J<sub>HH</sub> ~ 7.5 Hz, 4 CH<sub>Ph</sub>), 7.04 (m, 3 H, 1 CH<sub>Ph</sub> + 2 CH<sub>Xyl</sub>), 6.95 (d, 1 H, <sup>3</sup>J<sub>HH</sub> ~ 7.5 Hz, 1 CH<sub>Xyl</sub>), 6.79, 6.33, 5.81 (m, d, d, 1 H each, <sup>3</sup>J<sub>HH</sub> ~ 7.5 Hz, 3 CH<sub>Pyr</sub>), 2.70, 2.18 (s, 3 H each, 2 Me<sub>Xyl</sub>), 1.10 (s, 15 H, 5 Me<sub>Cp\*</sub>). <sup>13</sup>C{<sup>1</sup>H} NMR (C<sub>6</sub>D<sub>6</sub>, 25 °C):  $\delta$  170.4, 158.1 (C<sub>q-Pyr</sub>), 147.9 (C<sub>q-Ph</sub>), 140.4, 139.2, 136.6 (C<sub>q-Xyl</sub>), 137.4, 108.8, 105.0 (CH<sub>Pyr</sub>), 129.1, 125.3, 122.2 (2:2:1, CH<sub>Ph</sub>), 128.2, 127.9, 126.8 (CH<sub>Xyl</sub>), 91.9 (d, <sup>1</sup>J<sub>Crh</sub> = 8 Hz, C<sub>q-Cp\*</sub>), 21.9, 20.8 (Me<sub>Xyl</sub>), 8.8 (Me<sub>Cp\*</sub>). Elem anal. Calcd for C<sub>29</sub>H<sub>32</sub>ClRhN<sub>2</sub>: C, 63.7; H, 5.9; N, 5.1. Found: C, 63.7; H, 6.0; N, 5.2.

**Compound [3-Ir]BAR<sub>F</sub>.** To a solution of **2-Ir** (1.5 g, 2.36 mmol) in CH<sub>2</sub>Cl<sub>2</sub> (40 mL) was added NaBAR<sub>F</sub> (2.1 g, 2.36 mmol) in CH<sub>2</sub>Cl<sub>2</sub> (25 mL). Immediately the solution turned from orange to dark gray as a consequence of the formation of the cationic complex. The resulting mixture was filtered through Celite and evaporated to dryness and the residue washed with pentane to yield quantitatively the desired product. An analytically pure sample was obtained by crystallization from solutions in hexane–ether mixtures at −23 °C. Yield: 2.8 g (80%). <sup>1</sup>H NMR (CD<sub>2</sub>Cl<sub>2</sub>, 25 °C):  $\delta$  7.65 (t, 1 H, <sup>3</sup>J<sub>HH</sub> = 8.0 Hz, 1 CH<sub>Pyr</sub>), 7.44 (t, 2 H, <sup>3</sup>J<sub>HH</sub> = 7.7 Hz, 2 CH<sub>Ph</sub>), 7.33 (t, 1 H, <sup>3</sup>J<sub>HH</sub> = 7.6 Hz, 1 CH<sub>Xyl</sub>), 7.19 (m, 3 H, 1 CH<sub>Ph</sub> + 2 CH<sub>Xyl</sub>), 7.08 (d, 2 H, <sup>3</sup>J<sub>HH</sub> = 7.8 Hz, 2 CH<sub>Ph</sub>), 6.36, 5.89 (br s, 1 H each, 2 CH<sub>Pyr</sub>), 2.25 (s, 6 H, 2 Me<sub>Xyl</sub>), 1.31 (s, 15 H, 5 Me<sub>Cp\*</sub>). <sup>13</sup>C{<sup>1</sup>H} NMR (CD<sub>2</sub>Cl<sub>2</sub>, 25 °C):  $\delta$  178.3, 155.8 (br, C<sub>q-Pyr</sub>), 145.1, 119.5, 104.9 (br, CH<sub>Pyr</sub>), 143.5 (br, C<sub>q-Ph</sub>), 136.8, 135.9 (1:2, C<sub>q-Xyl</sub>), 130.5, 128.6 (1:2, CH<sub>Xyl</sub>), 129.9, 128.1, 123.1 (br, 2:1:2, CH<sub>Ph</sub>), 88.1 (C<sub>q-Cp\*</sub>), 20.6 (Me<sub>Xyl</sub>), 10.2 (Me<sub>Cp\*</sub>). HRMS (FAB). Calcd for C<sub>29</sub>H<sub>32</sub>N<sub>2</sub>Ir ([M]<sup>+</sup>): *m/z* 601.2195. Found: *m/z* 601.2202.

**Compound [3-Rh]BAR<sub>F</sub>.** Following the procedure described above for **[3-Ir]BAR<sub>F</sub>** but using **2-Rh**, complex **[3-Rh]BAR<sub>F</sub>** was obtained in quantitative spectroscopic yield. <sup>1</sup>H NMR (CD<sub>2</sub>Cl<sub>2</sub>, 25 °C):  $\delta$  7.44 (m, 3 H, 1 CH<sub>Pyr</sub> + 2 CH<sub>Ph</sub>), 7.36, 7.26 (t, d, 1:2, <sup>3</sup>J<sub>HH</sub> ~ 7.5 Hz, 3 CH<sub>Xyl</sub>), 7.22 (m, 3 H, 3 CH<sub>Ph</sub>), 6.33, 6.07 (d, 1 H each, <sup>3</sup>J<sub>HH</sub> ~ 7.5 Hz, 2 CH<sub>Pyr</sub>), 2.32 (s, 6 H, 2 Me<sub>Xyl</sub>), 1.34 (s, 15 H, 5 Me<sub>Cp\*</sub>). <sup>13</sup>C{<sup>1</sup>H} NMR (CD<sub>2</sub>Cl<sub>2</sub>, 25 °C):  $\delta$  175.3, 157.5 (C<sub>q-Pyr</sub>), 145.6 (C<sub>q-Ph</sub>), 143.5, 116.5, 104.2

(CH<sub>pyr</sub>), 137.9, 136.4 (1:2, C<sub>q-Xyl</sub>), 130.2, 123.2 (2:3, CH<sub>ph</sub>), 130.1, 128.6 (1:2, CH<sub>Xyl</sub>), 95.2 (d, <sup>1</sup>J<sub>CRh</sub> ~ 8 Hz, C<sub>q-Cp\*</sub>), 20.8 (Me<sub>Xyl</sub>), 9.6 (Me<sub>Cp\*</sub>). HRMS (FAB). Calcd for C<sub>29</sub>H<sub>32</sub>N<sub>2</sub>Rh ([M]<sup>+</sup>): *m/z* 511.1621. Found: *m/z* 511.1619.

**Compound [4-Ir]BAR<sub>F</sub>**. CO(g) was bubbled through a solution of compound [3-Ir]BAR<sub>F</sub> (0.2 g, 0.14 mmol) in CH<sub>2</sub>Cl<sub>2</sub> (5 mL) at room temperature for 5 min. During this period of time, the color of the solution changed from dark gray to bright orange. The resulting mixture was stirred for 10 min, and the volatiles were then removed under reduced pressure. <sup>1</sup>H NMR analysis of the crude product revealed quantitative conversion into the desired complex, which was crystallized from CH<sub>2</sub>Cl<sub>2</sub>–pentane mixtures at –23 °C. Yield: 60%. IR (Nujol):  $\nu(\text{CO})$  2048 cm<sup>-1</sup>. <sup>1</sup>H NMR (CD<sub>2</sub>Cl<sub>2</sub>, 25 °C):  $\delta$  7.59 (m, 1 H, 1 CH<sub>pyr</sub>), 7.40 (t, 2 H, <sup>3</sup>J<sub>HH</sub> = 7.7 Hz, 2 CH<sub>ph</sub>), 7.33 (t, 1 H, <sup>3</sup>J<sub>HH</sub> = 7.6 Hz, 1 CH<sub>Xyl</sub>), 7.19 (m, 3 H, 2 CH<sub>Xyl</sub> + 1 CH<sub>ph</sub>), 7.02 (d, 2 H, <sup>3</sup>J<sub>HH</sub> = 7.8 Hz, 2 CH<sub>ph</sub>), 6.53 (d, 1 H, <sup>3</sup>J<sub>HH</sub> = 8.8 Hz, 1 CH<sub>pyr</sub>), 6.42 (d, 1 H, <sup>3</sup>J<sub>HH</sub> = 7.3 Hz, 1 CH<sub>pyr</sub>), 2.19 (s, 6 H, 2 Me<sub>Xyl</sub>), 1.59 (s, 15 H, 5 Me<sub>Cp\*</sub>). <sup>13</sup>C{<sup>1</sup>H} NMR (CD<sub>2</sub>Cl<sub>2</sub>, 25 °C):  $\delta$  174.4, 157.0 (C<sub>q-pyr</sub>), 168.8 (IrCO), 141.9 (C<sub>q-ph</sub>), 140.8, 112.8, 107.9 (CH<sub>pyr</sub>), 137.1, 136.3, 136.2 (C<sub>q-Xyl</sub>), 130.3, 125.1, 123.7 (2:1:2, CH<sub>ph</sub>), 130.3, 128.7, 128.5 (CH<sub>Xyl</sub>), 101.6 (C<sub>q-Cp\*</sub>), 21.3, 20.4 (Me<sub>Xyl</sub>), 9.3 (Me<sub>Cp\*</sub>). Elem anal. Calcd for C<sub>62</sub>H<sub>44</sub>BF<sub>24</sub>IrN<sub>2</sub>O: C, 49.9; H, 3.0; N, 1.9. Found: C, 49.6; H, 3.0; N, 1.8.

**Compound [4-Rh]BAR<sub>F</sub>**. Following the procedure described above for [4-Ir]BAR<sub>F</sub> but using [3-Rh]BAR<sub>F</sub>, compound [4-Rh]BAR<sub>F</sub> was obtained in quantitative spectroscopic yield (the color of the solution changed from dark brown to orange) and was crystallized from CH<sub>2</sub>Cl<sub>2</sub>–pentane mixtures at –23 °C. Yield: 50%. IR (Nujol):  $\nu(\text{CO})$  2077 cm<sup>-1</sup>,  $\nu(\text{CO}_{\text{amide}})$  1687 cm<sup>-1</sup>. <sup>1</sup>H NMR (CD<sub>2</sub>Cl<sub>2</sub>, 25 °C):  $\delta$  7.77, 7.00, 6.66 (t, d, d, 1 H each, <sup>3</sup>J<sub>HH</sub> ~ 7.5 Hz, 3 CH<sub>pyr</sub>), 7.63, 7.23 (m, br, d, 3:1, <sup>3</sup>J<sub>HH</sub> ~ 7.5 Hz, 4 CH<sub>ph</sub>), 7.40 (t, 1 H, <sup>3</sup>J<sub>HH</sub> ~ 7.5 Hz, 1 CH<sub>Xyl</sub>), 7.28 (m, 3 H, 2 CH<sub>Xyl</sub> + 1 CH<sub>ph</sub>), 2.20, 2.12 (s, 3 H each, 2 Me<sub>Xyl</sub>), 1.59 (s, 15 H, 5 Me<sub>Cp\*</sub>). <sup>13</sup>C{<sup>1</sup>H} NMR (CD<sub>2</sub>Cl<sub>2</sub>, 25 °C):  $\delta$  189.3, 187.1 (d, <sup>1</sup>J<sub>CRh</sub> = 30 Hz, <sup>1</sup>J<sub>CRh</sub> = 76 Hz, RhCON and RhCO, respectively), 162.7, 158.7 (C<sub>q-pyr</sub>), 141.4, 123.4, 111.2 (CH<sub>pyr</sub>), 138.7, 137.2, 137.0 (C<sub>q-Xyl</sub>), 136.5 (C<sub>q-ph</sub>), 131.3, 131.2, 130.8, 129.3, 129.0 (CH<sub>ph</sub>), 130.6, 129.4 (1:2, CH<sub>Xyl</sub>), 109.3 (d, <sup>1</sup>J<sub>CRh</sub> = 5 Hz, C<sub>q-Cp\*</sub>), 22.3, 21.7 (Me<sub>Xyl</sub>), 9.5 (Me<sub>Cp\*</sub>). Elem anal. Calcd for C<sub>63</sub>H<sub>44</sub>BF<sub>24</sub>N<sub>2</sub>O<sub>2</sub>Rh: C, 52.9; H, 3.1; N, 2.0. Found: C, 53.3; H, 3.2; N, 1.8. HRMS (FAB). Calcd for C<sub>31</sub>H<sub>32</sub>N<sub>2</sub>O<sub>2</sub>Rh ([M]<sup>+</sup>): *m/z* 567.1519. Found: *m/z* 567.1503.

**Compound [5-Ir]BAR<sub>F</sub>**. C<sub>2</sub>H<sub>4</sub>(g) was bubbled through a solution of compound [3-Ir]BAR<sub>F</sub> (0.02 g, 0.014 mmol) in CH<sub>2</sub>Cl<sub>2</sub> (3 mL) in a Young NMR tube for 3 min. During this period of time, the color of the solution changed from black to orange. <sup>1</sup>H NMR analysis of the crude product revealed quantitative conversion into complex [5-Ir]BAR<sub>F</sub> in an admixture with free ethylene. This complex could not be isolated because of its reversion to the starting material in the absence of C<sub>2</sub>H<sub>4</sub> and to its evolution at room temperature to 6-Ir<sup>+</sup>. <sup>1</sup>H NMR (CD<sub>2</sub>Cl<sub>2</sub>, –40 °C):  $\delta$  7.44 (t, 1 H, <sup>3</sup>J<sub>HH</sub> = 8.1 Hz, 1 CH<sub>pyr</sub>), 7.34 (t, 2 H, <sup>3</sup>J<sub>HH</sub> = 7.1 Hz, 2 CH<sub>ph</sub>), 7.28, 7.17 (m, 1:2, 3 CH<sub>Xyl</sub>), 7.09 (t, 1 H, <sup>3</sup>J<sub>HH</sub> = 7.4 Hz, 1 CH<sub>ph</sub>), 7.00 (d, 2 H, <sup>3</sup>J<sub>HH</sub> = 7.9 Hz, 2 CH<sub>ph</sub>), 6.50 (d, 1 H, <sup>3</sup>J<sub>HH</sub> = 8.9 Hz, 1 CH<sub>pyr</sub>), 6.24 (d, 1 H, <sup>3</sup>J<sub>HH</sub> = 7.2 Hz, 1 CH<sub>pyr</sub>), 4.02 (br, d, 4 H, <sup>3</sup>J<sub>HH</sub> = 8.6 Hz, IrC<sub>2</sub>H<sub>4</sub>), 2.15, 2.06 (s, 3 H each, 2 Me<sub>Xyl</sub>), 1.34 (s, 15 H, 5 Me<sub>Cp\*</sub>). <sup>13</sup>C{<sup>1</sup>H} NMR (CD<sub>2</sub>Cl<sub>2</sub>, –40 °C):  $\delta$  171.0, 156.6 (C<sub>q-pyr</sub>), 141.7 (C<sub>q-ph</sub>), 139.1, 111.4, 108.0 (CH<sub>pyr</sub>), 137.1, 136.3, 135.2 (C<sub>q-Xyl</sub>), 129.5, 123.4, 122.2 (2:1:2, CH<sub>ph</sub>), 129.4, 128.1, 127.5 (CH<sub>Xyl</sub>), 98.5 (C<sub>q-Cp\*</sub>), 61.7 (IrC<sub>2</sub>H<sub>4</sub>), 21.8, 20.9 (Me<sub>Xyl</sub>), 8.5 (Me<sub>Cp\*</sub>).

**Compound [6-Ir]BAR<sub>F</sub>**. C<sub>2</sub>H<sub>4</sub>(g) was bubbled through a solution of compound [3-Ir]BAR<sub>F</sub> (0.1 g, 0.068 mmol) in CH<sub>2</sub>Cl<sub>2</sub> (15 mL) for 3 min. The resulting mixture was stirred for 24 h. The color changed from orange to green, and then the volatiles were removed under reduced pressure. Quantitative conversion into [6-Ir]BAR<sub>F</sub> was ascertained by <sup>1</sup>H NMR, and the product was crystallized from Et<sub>2</sub>O–pentane mixtures at –23 °C. Yield: 78 mg (75%). IR (Nujol):  $\nu(\text{Ir–H})$  2096 cm<sup>-1</sup>. <sup>1</sup>H NMR (CD<sub>2</sub>Cl<sub>2</sub>, 25 °C):  $\delta$  7.73–7.67 (m, 5 H, 5 CH<sub>ph</sub>), 7.60 (t, 1 H, <sup>3</sup>J<sub>HH</sub> = 8.0 Hz, 1 CH<sub>pyr</sub>), 7.34 (t, 1 H, <sup>3</sup>J<sub>HH</sub> = 7.1 Hz, 1 CH<sub>Xyl</sub>), 7.25 (m, 2 H, 2 CH<sub>Xyl</sub>), 6.93 (dd, 1 H, <sup>3</sup>J<sub>HH</sub> = 7.5 Hz, <sup>4</sup>J<sub>HH</sub> = 1.5 Hz, 1 CH<sub>pyr</sub>), 6.84 (dd, 1 H, <sup>3</sup>J<sub>HH</sub> = 8.5 Hz, <sup>4</sup>J<sub>HH</sub> = 1.5 Hz, 1 CH<sub>pyr</sub>), 2.69 (d, 3 H, <sup>4</sup>J<sub>HH</sub> = 2.3 Hz, Ir=CMe), 2.10, 2.06 (s, 3 H each, 2 Me<sub>Xyl</sub>), 1.65 (s, 15 H, 5 Me<sub>Cp\*</sub>), –16.42 (br, s, 1 H, IrH). <sup>13</sup>C{<sup>1</sup>H} NMR (CD<sub>2</sub>Cl<sub>2</sub>, 25 °C):  $\delta$  235.9 (Ir=CMe), 165.9, 160.6 (C<sub>q-pyr</sub>), 139.7

(C<sub>q-ph</sub>), 139.4, 137.7, 137.3 (C<sub>q-Xyl</sub>), 138.2, 124.6, 113.9 (CH<sub>pyr</sub>), 131.8, 131.4, 127.6 (2:1:2, CH<sub>ph</sub>), 130.4, 129.2 (1:2, CH<sub>Xyl</sub>), 98.4 (C<sub>q-Cp\*</sub>), 35.4 (Ir=CMe), 21.5, 19.7 (Me<sub>Xyl</sub>), 9.8 (Me<sub>Cp\*</sub>). Elem anal. Calcd for C<sub>63</sub>H<sub>48</sub>BF<sub>24</sub>IrN<sub>2</sub>: C, 50.7; H, 3.2; N, 1.9. Found: C, 50.6; H, 3.5; N, 1.7.

**Compound [7-Ir]BAR<sub>F</sub>**. To a solution of compound [6-Ir]BAR<sub>F</sub> (0.02 g, 0.013 mmol) in CD<sub>2</sub>Cl<sub>2</sub> (0.5 mL) in a Young NMR tube was added an excess of PMe<sub>3</sub> (0.05 mL, 0.5 mmol). <sup>1</sup>H NMR analysis of the crude product revealed quantitative conversion into complex [7-Ir]BAR<sub>F</sub> after 15 h at room temperature. Free trimethylphosphine was removed under reduced pressure, and compound [7-Ir]BAR<sub>F</sub> was crystallized from CH<sub>2</sub>Cl<sub>2</sub>–pentane mixtures at –23 °C. Yield: 15 mg (70%). <sup>1</sup>H NMR (CD<sub>2</sub>Cl<sub>2</sub>, –40 °C):  $\delta$  7.49, 7.31 (t, m, 2:3, <sup>3</sup>J<sub>HH</sub> ~ 7.5 Hz, 3 CH<sub>ph</sub>), 7.35, 6.50, 6.21 (t, d, d, 1 H each, <sup>3</sup>J<sub>HH</sub> ~ 7.5 Hz, 3 CH<sub>pyr</sub>), 7.15, 7.06 (m, 1:2, 3 CH<sub>Xyl</sub>), 3.67 (m, 2 H, 1 IrCH<sub>2</sub>CH<sub>2</sub>), 2.09 (s, 6 H, 2 Me<sub>Xyl</sub>), 1.62 (s, 15 H, 5 Me<sub>Cp\*</sub>), 1.47 (m, 2 H, 1 IrCH<sub>2</sub>CH<sub>2</sub>), 1.38 (d, 18 H, <sup>2</sup>J<sub>HP</sub> = 9.5 Hz, 2 PMe<sub>3</sub>). <sup>13</sup>C{<sup>1</sup>H} NMR (CD<sub>2</sub>Cl<sub>2</sub>, 25 °C):  $\delta$  158.6, 158.3 (C<sub>q-pyr</sub>), 145.4 (C<sub>q-ph</sub>), 142.5, 136.3, 127.4 (C<sub>q-Xyl</sub>), 131.0, 129.8 (2:3, CH<sub>ph</sub>), 128.1, 127.9 (1:2, CH<sub>Xyl</sub>), 126.8, 113.4, 106.9 (CH<sub>pyr</sub>), 99.0 (C<sub>q-Cp\*</sub>), 56.0 (t, <sup>3</sup>J<sub>CP</sub> = 5 Hz, IrCH<sub>2</sub>CH<sub>2</sub>), 20.7 (Me<sub>Xyl</sub>), 18.1 (d, <sup>1</sup>J<sub>CP</sub> = 38 Hz, PMe<sub>3</sub>), 10.1 (Me<sub>Cp\*</sub>), –7.1 (t, <sup>3</sup>J<sub>CP</sub> = 7 Hz, IrCH<sub>2</sub>CH<sub>2</sub>). <sup>31</sup>P{<sup>1</sup>H} NMR (160 MHz, CD<sub>2</sub>Cl<sub>2</sub>, 25 °C):  $\delta$  –45.4.

**Compound [8-Ir]BAR<sub>F</sub>**. A solution of complex [3-Ir]BAR<sub>F</sub> (0.05 g, 0.034 mmol) in CH<sub>2</sub>Cl<sub>2</sub> (1.25 mL) was treated with H<sub>2</sub> (1 atm), and the resulting mixture was stirred for 10 min at room temperature. <sup>1</sup>H NMR analysis of the reaction mixture revealed the formation of complex [8-Ir]BAR<sub>F</sub> together with its isomer [3-Ir]BAR<sub>F</sub> in a ca. 3:1 ratio. [8-Ir]BAR<sub>F</sub> was separated by fractional crystallization from CH<sub>2</sub>Cl<sub>2</sub>–pentane mixtures at –23 °C as bright-orange crystals. Yield: 10 mg (22%). <sup>1</sup>H NMR (CD<sub>2</sub>Cl<sub>2</sub>, 25 °C):  $\delta$  7.71 (br, s, 1 H, 1 CH<sub>Xyl</sub>), 7.69 (m, 1 H, 1 CH<sub>pyr</sub>), 7.50 (t, 2 H, <sup>3</sup>J<sub>HH</sub> = 7.8 Hz, 2 CH<sub>ph</sub>), 7.46 (m, 1 H, 1 CH<sub>Xyl</sub>), 7.33 (t, 1 H, <sup>3</sup>J<sub>HH</sub> = 7.5 Hz, 1 CH<sub>ph</sub>), 7.24 (d, 2 H, <sup>3</sup>J<sub>HH</sub> = 7.8 Hz, 2 CH<sub>ph</sub>), 6.98 (d, 1 H, <sup>3</sup>J<sub>HH</sub> = 8.4 Hz, 1 CH<sub>Xyl</sub>), 6.93 (d, 1 H, <sup>3</sup>J<sub>HH</sub> = 8.7 Hz, 1 CH<sub>pyr</sub>), 6.25 (br, s, 1 H, NH), 6.23 (d, 1 H, <sup>3</sup>J<sub>HH</sub> = 7.7 Hz, 1 CH<sub>pyr</sub>), 3.61, 2.11 (d, 1 H each, <sup>2</sup>J<sub>HP</sub> = 4.8 Hz, IrCH<sub>2</sub>), 2.47 (s, 3 H, 1 Me<sub>Xyl</sub>), 1.58 (s, 15 H, 5 Me<sub>Cp\*</sub>). <sup>13</sup>C{<sup>1</sup>H} NMR (CD<sub>2</sub>Cl<sub>2</sub>, 25 °C):  $\delta$  154.5, 154.0 (C<sub>q-pyr</sub>), 141.4, 118.8, 108.8 (CH<sub>pyr</sub>), 137.8 (C<sub>q-Xyl</sub>), 136.9 (C<sub>q-ph</sub>), 134.0, 130.4, 129.5 (CH<sub>Xyl</sub>), 130.8, 126.8, 122.8 (2:1:2, CH<sub>ph</sub>), 100.8 (IrCH<sub>2</sub>C<sub>q</sub>), 93.9 (IrC<sub>q-Xyl</sub>), 90.3 (C<sub>q-Cp\*</sub>), 35.6 (IrCH<sub>2</sub>), 20.8 (Me<sub>Xyl</sub>), 9.3 (Me<sub>Cp\*</sub>). HRMS (FAB). Calcd for C<sub>29</sub>H<sub>32</sub>N<sub>2</sub>Ir ([M]<sup>+</sup>): *m/z* 601.2195. Found: *m/z* 601.2181. Elem anal. Calcd for C<sub>61</sub>H<sub>44</sub>BF<sub>24</sub>IrN<sub>2</sub>: C, 50.0; H, 3.0; N, 1.9. Found: C, 49.8; H, 3.1; N, 1.8.

**Compound [8-Rh]BAR<sub>F</sub>**. In a Young NMR tube, a solution of complex [3-Rh]BAR<sub>F</sub> (40 mg, 0.029 mmol) in CH<sub>2</sub>Cl<sub>2</sub> (0.5 mL) was treated with H<sub>2</sub> (60 mol %), and after 24 h at room temperature, <sup>1</sup>H NMR analysis of the reaction mixture revealed transformation into complex [8-Rh]BAR<sub>F</sub> in 50% spectroscopic yield. [8-Rh]BAR<sub>F</sub> was separated by fractional crystallization from CH<sub>2</sub>Cl<sub>2</sub>–pentane mixtures at –23 °C as bright-red crystals. Yield: 16 mg (38%). IR (Nujol):  $\nu(\text{NH})$  3396 cm<sup>-1</sup>. <sup>1</sup>H NMR (CD<sub>2</sub>Cl<sub>2</sub>, 25 °C):  $\delta$  7.73 (br, s, 1 H, 1 CH<sub>Xyl</sub>, detected by NOESY experiment, under the BAR<sub>F</sub><sup>–</sup> signal), 7.63, 6.90, 6.30 (t, d, d, 1 H each, <sup>3</sup>J<sub>HH</sub> ~ 7.5 Hz, 3 CH<sub>pyr</sub>), 7.49 (m, 3 H, 1 CH<sub>Xyl</sub> + 2 CH<sub>ph</sub>), 7.31, 7.25 (t, d, 1:2, <sup>3</sup>J<sub>HH</sub> ~ 7.5 Hz, 3 CH<sub>ph</sub>), 6.97 (d, 1 H, <sup>3</sup>J<sub>HH</sub> ~ 7.5 Hz, 1 CH<sub>Xyl</sub>), 6.14 (br, s, 1 H, NH), 3.64, 2.54 (d, 1 H each, <sup>2</sup>J<sub>HP</sub> ~ 3.5 Hz, RhCH<sub>2</sub>), 2.48 (s, 3 H, 1 Me<sub>Xyl</sub>), 1.51 (s, 15 H, 5 Me<sub>Cp\*</sub>). <sup>13</sup>C{<sup>1</sup>H} NMR (CD<sub>2</sub>Cl<sub>2</sub>, 25 °C):  $\delta$  155.6, 153.8 (C<sub>q-pyr</sub>), 141.4, 117.5, 109.1 (CH<sub>pyr</sub>), 137.9 (C<sub>q-Xyl</sub>), 137.3 (C<sub>q-ph</sub>), 133.5, 131.0, 129.0 (CH<sub>Xyl</sub>), 130.8, 126.6, 122.6 (2:1:2, CH<sub>ph</sub>), 107.3 (br, RhCH<sub>2</sub>C<sub>q-Xyl</sub>, detected by HMBC experiment), 100.6 (br, RhC<sub>q-Xyl</sub>), 96.7 (d, <sup>1</sup>J<sub>CRh</sub> = 7.3 Hz, C<sub>q-Cp\*</sub>), 47.9 (d, <sup>1</sup>J<sub>CRh</sub> = 13.8 Hz, RhCH<sub>2</sub>), 20.8 (Me<sub>Xyl</sub>), 9.5 (Me<sub>Cp\*</sub>). HRMS (FAB). Calcd for C<sub>29</sub>H<sub>32</sub>N<sub>2</sub>Rh ([M]<sup>+</sup>): *m/z* 511.1621. Found: *m/z* 511.1620.

**Observation of a Hydride Intermediate in the Reaction of [3-Ir]BAR<sub>F</sub> with H<sub>2</sub>**. In a Young NMR tube, a solution of complex [3-Ir]BAR<sub>F</sub> (0.02 g, 14  $\mu$ mol) in CD<sub>2</sub>Cl<sub>2</sub> (0.5 mL) was treated with H<sub>2</sub> (500 mol %), and after 1–2 min at room temperature, the solution color changed from dark gray to orange. <sup>1</sup>H NMR analysis of the reaction mixture revealed the formation of a hydride intermediate in  $\geq$ 95% spectroscopic yield. This complex could not be isolated or be completely characterized (see the text). <sup>1</sup>H NMR (CD<sub>2</sub>Cl<sub>2</sub>, 25 °C):  $\delta$  8.03 (t, 1 H, <sup>3</sup>J<sub>HH</sub> = 7.9 Hz, 1 CH<sub>Ar</sub>), 7.53–6.85 (10 CH<sub>Ar</sub>), 2.12 (s, 6 H, 2 Me<sub>Xyl</sub>),

1.20 (s, 15 H, 5 Me<sub>Cp\*</sub>), −6.32 (s, 1 H, IrH). A resonance attributable to a possible NH proton could not be located.

**Compound [9-Ir]BAR<sub>F</sub>.** CO(g) was bubbled through a solution of compound [8-Ir]BAR<sub>F</sub> (0.01 g, 6.8 μmol) in CH<sub>2</sub>Cl<sub>2</sub> (2.5 mL) at room temperature for 5 min. The solution changed color immediately from orange to light yellow. The solvent was removed under reduced pressure, and <sup>1</sup>H NMR analysis of the reaction product showed quantitative conversion into [9-Ir]BAR<sub>F</sub>. It was washed with pentane and dried under vacuum. IR (Nujol): ν(NH) 3356 cm<sup>−1</sup>, ν(CO) 2029 cm<sup>−1</sup>. <sup>1</sup>H NMR (CD<sub>2</sub>Cl<sub>2</sub>, 25 °C): δ 7.64, 6.87 (t, d, 1 H each, <sup>3</sup>J<sub>HH</sub> ~ 7.5 Hz, 2 CH<sub>Pyr</sub>), 7.54, 7.42 (m, t, 2:1, <sup>3</sup>J<sub>HH</sub> = 7.5 Hz, 3 CH<sub>Ph</sub>), 7.30 (m, 3 H, 2 CH<sub>Ph</sub> + 1 CH<sub>Xyl</sub>), 7.19 (m, 3 H, 1 CH<sub>Xyl</sub> + 1 CH<sub>Pyr</sub> + NH), 7.10 (d, 1 H, <sup>3</sup>J<sub>HH</sub> = 7.5 Hz, 1 CH<sub>Xyl</sub>), 3.73, 2.99 (d, 1 H each, <sup>2</sup>J<sub>HH</sub> = 11.0 Hz, IrCH<sub>2</sub>), 2.32 (s, 3 H, 1 Me<sub>Xyl</sub>), 1.67 (s, 15 H, 5 Me<sub>Cp\*</sub>). <sup>13</sup>C{<sup>1</sup>H} NMR (CD<sub>2</sub>Cl<sub>2</sub>, 25 °C): δ 168.1 (CO), 159.7, 155.2 (C<sub>q-Pyr</sub>), 144.6 (C<sub>q-Ph</sub>), 140.4, 118.6, 108.4 (CH<sub>Pyr</sub>), 138.1, 137.9, 137.5 (C<sub>q-Xyl</sub>), 131.1, 128.2, 125.3 (2:1:2, CH<sub>Ph</sub>), 129.9, 129.3, 123.6 (CH<sub>Xyl</sub>), 101.9 (C<sub>q-Cp\*</sub>), 21.9 (Me<sub>Xyl</sub>), 8.9 (IrCH<sub>2</sub>), 8.8 (Me<sub>Cp\*</sub>). Elem. anal. Calcd for C<sub>62</sub>H<sub>44</sub>BF<sub>24</sub>IrN<sub>2</sub>O: C, 49.9; H, 3.0; N, 1.9. Found: C, 49.7; H, 3.4; N, 1.6.

**Computational Details.** DFT calculations were carried out with the *Gaussian 09* program.<sup>39</sup> Geometry optimizations of all species were calculated in the gas phase without restrictions using the PBE0 functional.<sup>40</sup> All light atoms were represented with the 6-31g(d,p) basis set, while the iridium and rhodium atoms were described by the SDD basis set and its associated electron core potential.<sup>41</sup> Frequency calculations were performed on the optimized structures at the same level of theory to characterize the stationary points, as well as for calculation of the gas-phase enthalpies (*H*), entropies (*S*), and Gibbs energies (*G*). The nature of the intermediates connected by a transition state was determined by intrinsic reaction coordinate (IRC) calculations or by perturbation of the transition states along the transition-state coordinate and optimization to a minimum. Bulk solvent effects were modeled using Truhlar's SMD continuum solvent model,<sup>42</sup> and empirical dispersion corrections were added with the D3 version of Grimme's dispersion.<sup>43–45</sup> Both corrections were made on the gas-phase geometries by single-point calculations. All energies reported throughout the text are zero-point-corrected potential energies in dichloromethane.

## ■ ASSOCIATED CONTENT

### Supporting Information

The Supporting Information is available free of charge on the ACS Publications website at DOI: 10.1021/acs.inorgchem.7b02283.

Experimental procedures for the synthesis of compounds **1** and [5-Rh]BAR<sub>F</sub>, proposed mechanism for the H<sub>2</sub>-catalyzed isomerization between 3-M<sup>+</sup> and 8-M<sup>+</sup>, NMR spectra of all compounds, crystallographic data and details of the structure determinations for 2-Ir, 2-Rh, [3-Ir]BAR<sub>F</sub>, [4-Ir]BAR<sub>F</sub>, [4-Rh]BAR<sub>F</sub>, [5-Rh]BAR<sub>F</sub>, [6-Ir]BAR<sub>F</sub>, [7-Ir]BAR<sub>F</sub>, [8-Ir]BAR<sub>F</sub>, and [8-Rh]BAR<sub>F</sub>, and additional computational details (PDF)

Geometric coordinates of all transition states and intermediates (XYZ)

### Accession Codes

CCDC 1572330–1572339 contain the supplementary crystallographic data for this paper. These data can be obtained free of charge via [www.ccdc.cam.ac.uk/data\\_request/cif](http://www.ccdc.cam.ac.uk/data_request/cif), or by emailing [data\\_request@ccdc.cam.ac.uk](mailto:data_request@ccdc.cam.ac.uk), or by contacting The Cambridge Crystallographic Data Centre, 12 Union Road, Cambridge CB2 1EZ, UK; fax: +44 1223 336033.

## ■ AUTHOR INFORMATION

### Corresponding Author

\*E-mail: [nuria@iiq.csic.es](mailto:nuria@iiq.csic.es) (N.R.). Fax: (+34)954460565.

### ORCID

Nuria Rendón: 0000-0003-1760-185X

Joaquín López-Serrano: 0000-0003-3999-0155

### Author Contributions

The manuscript was written through contributions of all authors. All authors have given approval to the final version of the manuscript.

### Notes

The authors declare no competing financial interest.

## ■ ACKNOWLEDGMENTS

Financial support (FEDER contribution) from the Spanish Ministerio de Economía y Competitividad (Projects CTQ2016-80814-R, CTQ2016-75193-P, and CTQ2016-81797-REDC) and Junta de Andalucía (Grant FQM-119) is acknowledged. The use of computational facilities of The Supercomputing Center of Galicia (CESGA) is thankfully acknowledged.

## ■ DEDICATION

Dedicated to Prof. Peter M. Maitlis on the occasion of his 85th birthday in recognition of his outstanding contributions to organometallic chemistry.

## ■ REFERENCES

- (1) (a) Valpuesta, J. E. V.; Rendón, N.; López-Serrano, J.; Poveda, M. L.; Sánchez, L.; Álvarez, E.; Carmona, E. Dihydrogen-Catalyzed Reversible Carbon–Hydrogen and Nitrogen–Hydrogen Bond Formation in Organometallic Iridium Complexes. *Angew. Chem., Int. Ed.* **2012**, *51*, 7555–7557. (b) Zamorano, A.; Rendón, N.; López-Serrano, J.; Valpuesta, J. E. V.; Álvarez, E.; Carmona, E. Dihydrogen Catalysis of the Reversible Formation and Cleavage of C–H and N–N Bonds of Aminopyridinate Ligands Bound to (η<sup>5</sup>-C<sub>5</sub>Me<sub>5</sub>)Ir<sup>III</sup>. *Chem. - Eur. J.* **2015**, *21*, 2576–2587.
- (2) Zamorano, A.; Rendón, N.; Valpuesta, J. E. V.; Álvarez, E.; Carmona, E. Synthesis and Reactivity toward H<sub>2</sub> of (η<sup>5</sup>-C<sub>5</sub>Me<sub>5</sub>)Rh(III) Complexes with Bulky Aminopyridinate Ligands. *Inorg. Chem.* **2015**, *54*, 6573–6581.
- (3) (a) Barr, D.; Clegg, W.; Mulvey, R. E.; Snaith, R. The Isolation and Crystal Structure of [Ph(Z-Pyr)NLi]·(HMPA)=[Ph(2-Pyr)NH]; a Model Monomeric Organonitrogen-Lithium Species containing Coordination of Lithium by both an Anchimeric Pyridyl N-Atom and by a Potentially Reactive Amine Ligand. *J. Chem. Soc., Chem. Commun.* **1984**, 469–470. (b) Scott, N. M.; Schareina, T.; Tok, O.; Kempe, R. Lithium and Potassium Amides of Sterically Demanding Aminopyridines. *Eur. J. Inorg. Chem.* **2004**, *2004*, 3297–3304. (c) Lyubov, D. M.; Doring, C.; Ketkov, S. Y.; Kempe, R.; Trifonov, A. A. Selective Protonation of the Y–C Bond in Trinuclear Yttrium Alkyl–Hydrido Clusters and Formation of the Cationic Polyhydrido Core. *Chem. - Eur. J.* **2011**, *17*, 3824–3826.
- (4) (a) Hintermair, U.; Sheehan, S. W.; Parent, A. R.; Ess, D. H.; Richens, D. T.; Vaccaro, P. H.; Brudvig, G. W.; Crabtree, R. H. Precursor Transformation during Molecular Oxidation Catalysis with Organometallic Iridium Complexes. *J. Am. Chem. Soc.* **2013**, *135*, 10837–10851. (b) Graepner, J.; Hintermair, U.; Huang, D. L.; Thomsen, J. M.; Takase, M.; Campos, J.; Hashmi, S. M.; Elimelech, M.; Brudvig, G. W.; Crabtree, R. H. Probing the Viability of Oxo-Coupling Pathways in Iridium-Catalyzed Oxygen Evolution. *Organometallics* **2013**, *32*, 5384–5390. (c) Hintermair, U.; Hashmi, S. M.; Elimelech, M.; Crabtree, R. H. Particle Formation during Oxidation Catalysis with Cp\* Iridium Complexes. *J. Am. Chem. Soc.* **2012**, *134*, 9785–9795. (d) Crabtree, R. H. An Organometallic Future in Green and Energy Chemistry? *Organometallics* **2011**, *30*, 17–19.
- (5) Zuccaccia, C.; Bellachioma, G.; Bortolini, G.; Bucci, A.; Savini, A.; Macchioni, A. Transformation of a Cp\*–Iridium(III) Precatalyst for Water Oxidation when Exposed to Oxidative Stress. *Chem. - Eur. J.* **2014**, *20*, 3446–3456.

(6) Kuwata, S.; Ikariya, T. Metal–ligand bifunctional reactivity and catalysis of protic N-heterocyclic carbene and pyrazole complexes featuring  $\beta$ -NH units. *Chem. Commun.* **2014**, *50*, 14290–14300.

(7) (a) Han, Y.-F.; Jin, G.-X. Cyclometalated  $[\text{Cp}^*\text{M}(\text{CX})]$  (M = Ir, Rh; X = N, C, O, P) complexes. *Chem. Soc. Rev.* **2014**, *43*, 2799–2823. (b) Wang, C.; Villa-Marcos, B.; Xiao, J. Hydrogenation of imino bonds with half-sandwich metal catalysts. *Chem. Commun.* **2011**, *47*, 9773–9785.

(8) Liu, Z.; Sadler, P. J. Organoiridium Complexes: Anticancer Agents and Catalysts. *Acc. Chem. Res.* **2014**, *47*, 1174–1185.

(9) Smith, D. P.; Chen, H.; Ogo, S.; Elduque, A. I.; Eisenstein, M.; Olmstead, M.; Fish, R. H. Bioorganometallic Chemistry. 27. Synthetic, X-ray Crystallographic, and Competitive Binding Studies in the Reactions of Nucleobases, Nucleosides, and Nucleotides with  $[\text{Cp}^*\text{Rh}(\text{H}_2\text{O})_3](\text{OTf})_2$ , as a Function of pH, and the Utilization of Several  $\text{Cp}^*\text{Rh}$ –DNA Base Complexes in Host–Guest Chemistry. *Organometallics* **2014**, *33*, 2389–2404.

(10) (a) Hartwig, J. *Organotransition Metal Chemistry. From Bonding to Catalysis*; University Science Books, 2010. (b) Bochmann, M. *Organometallics and Catalysis: An Introduction*; Oxford University Press, 2014.

(11) For example, see: (a) Nova, A.; Taylor, D. J.; Blacker, A. J.; Duckett, S. B.; Perutz, R. N.; Eisenstein, O. Computational Studies Explain the Importance of Two Different Substituents on the Chelating Bis(amido) Ligand for Transfer Hydrogenation by Bifunctional  $\text{Cp}^*\text{Rh}(\text{III})$  Catalysts. *Organometallics* **2014**, *33*, 3433–3442 and references cited therein. (b) Blacker, A. J.; Clot, E.; Duckett, S. B.; Eisenstein, O.; Grace, J.; Nova, A.; Perutz, R. N.; Taylor, D. J.; Whitwood, A. C. Synthesis and structure of “16-electron” rhodium(III) catalysts for transfer hydrogenation of a cyclic imine: mechanistic implications. *Chem. Commun.* **2009**, 6801–6803.

(12) (a) Hanley, P. S.; Hartwig, J. F. Migratory Insertion of Alkenes into Metal–Oxygen and Metal–Nitrogen Bonds. *Angew. Chem., Int. Ed.* **2013**, *52*, 8510–8525. (b) Tye, J. W.; Hartwig, J. F. Computational Studies of the Relative Rates for Migratory Insertions of Alkenes into Square-Planar, Methyl-, Amido-, and Hydroxo Complexes of Rhodium. *J. Am. Chem. Soc.* **2009**, *131*, 14703–14712.

(13) (a) Casalnuovo, A. L.; Calabrese, J. C.; Milstein, D. Rational design in homogeneous catalysis. Iridium(I)-catalyzed addition of aniline to norbornylene via nitrogen-hydrogen activation. *J. Am. Chem. Soc.* **1988**, *110*, 6738–6744. (b) Neukom, J. D.; Perch, N. S.; Wolfe, J. P. Intramolecular Alkene Aminopalladation Reactions of  $(\text{dppf})\text{Pd}(\text{Ar})\text{[N}(\text{Ar}^1)(\text{CH}_2)_3\text{CH}=\text{CH}_2]$  Complexes. Insertion of Unactivated Alkenes into Pd–N Bonds. *J. Am. Chem. Soc.* **2010**, *132*, 6276–6277. (c) White, P. B.; Stahl, S. S. Reversible Alkene Insertion into the Pd–N Bond of Pd(II)-Sulfonamides and Implications for Catalytic Amidation Reactions. *J. Am. Chem. Soc.* **2011**, *133*, 18594–18597.

(14) For the terminology employed to refer to complexes with carbene ligands, see: Peloso, R.; Carmona, E. Non-heteroatom-substituted alkylidene complexes of groups 10 and 11. *Coord. Chem. Rev.* **2017**, *10.1016/j.ccr.2017.07.018*. See also ref 10b.

(15) Heiden, Z. M.; Rauchfuss, T. B. Homogeneous Catalytic Reduction of Dioxygen Using Transfer Hydrogenation Catalysts. *J. Am. Chem. Soc.* **2007**, *129*, 14303–14310.

(16) (a) Holland, P. L.; Andersen, R. A.; Bergman, R. G. Synthesis, Characterization, Isomerization, and Reactivity of Dimeric Cyclopentadienylnickel Amido Complexes. *J. Am. Chem. Soc.* **1996**, *118*, 1092–1104. (b) Mindiola, D. J.; Hillhouse, G. L. Isocyanate and carbodiimide synthesis by nitrene-group-transfer from a nickel(II) imido complex. *Chem. Commun.* **2002**, 1840–1841. (c) Tomon, T.; Koizumi, T.-a.; Tanaka, K. Electrochemical Hydrogenation of  $[\text{Ru}(\text{bpy})_2(\text{napy-}\kappa\text{N})(\text{CO})]^{2+}$ : Inhibition of Reductive Ru–CO Bond Cleavage by a Ruthenacycle. *Angew. Chem., Int. Ed.* **2005**, *44*, 2229–2232. (d) Liang, L.-C.; Hung, Y.-T.; Huang, Y.-L.; Chien, P.-S.; Lee, P.-Y.; Chen, W.-C. Divergent Carbonylation Reactivity Preferences of Nickel Complexes Containing Amido Pincer Ligands: Migratory Insertion versus Reductive Elimination. *Organometallics* **2012**, *31*, 700–708. (e) Shishilov, O. N.; Kumanyaev, I. M.; Akhmadullina, N. S.; Churakov, A. V.; Garbuzova, I. A.; Flid, V. R. The first carbamoyl–

carboxylate complex of transition metals: Synthesis and structure of  $\{(\text{OC}_4\text{H}_8\text{NH})[\text{OC}_4\text{H}_8\text{NC}(\text{O})\text{Pd}]_2(\mu\text{-CMe}_3\text{CO}_2)_2\}$ . *Inorg. Chem. Commun.* **2015**, *58*, 16–19.

(17) Bassetti, M.; Monti, D.; Haynes, A.; Pearson, J. M.; Stanbridge, I. A.; Maitlis, P. M. Relative reaction rates for rhodium and iridium: oxidative addition of methyl iodide to M(I) and the migratory insertion in M(III) methyl carbonyl complexes. *Gazz. Chim. Ital.* **1992**, *122*, 391–393.

(18) Campos, J.; Carmona, E. Rhodium and Iridium Complexes of Bulky Tertiary Phosphine Ligands. Searching for Isolable Cationic  $\text{M}^{\text{III}}$  Alkylidenes. *Organometallics* **2015**, *34*, 2212–2221.

(19) (a) Lara, P.; Paneque, M.; Poveda, M. L.; Santos, L. L.; Valpuesta, J. E. V.; Carmona, E.; Moncho, S.; Ujaque, G.; Lledós, A.; Álvarez, E.; Mereiter, K. Experimental and Computational Studies on the Iridium Activation of Aliphatic and Aromatic C–H Bonds of Alkyl Aryl Ethers and Related Molecules. *Chem. - Eur. J.* **2009**, *15*, 9034–9045. (b) Paneque, M.; Poveda, M. L.; Santos, L. L.; Carmona, E.; Mereiter, K. Generation of Metallacyclic Structures from the Reactions of Vinyl Ethers with a  $\text{Tp}^{\text{Me}_2}\text{Ir}^{\text{III}}$  Compound. *Organometallics* **2008**, *27*, 6353–6359. (c) Paneque, M.; Poveda, M. L.; Rendón, N.; Álvarez, E.; Carmona, E. The Synthesis of Iridabenzenes by the Coupling of Iridacyclopentadienes and Olefins. *Eur. J. Inorg. Chem.* **2007**, *2007*, 2711–2720.

(20) Campos, J.; López-Serrano, J.; Álvarez, E.; Carmona, E. Cationic Ir(III) Alkylidenes Are Key Intermediates in C–H Bond Activation and C–C Bond-Forming Reactions. *J. Am. Chem. Soc.* **2012**, *134*, 7165–7175.

(21) (a) Lara, P.; Paneque, M.; Poveda, M. L.; Santos, L. L.; Valpuesta, J. E. V.; Salazar, V.; Carmona, E.; Moncho, S.; Ujaque, G.; Lledós, A.; Maya, C.; Mereiter, K. Synthetic, Mechanistic, and Theoretical Studies on the Generation of Iridium Hydride Alkylidene and Iridium Hydride Alkene Isomers. *Chem. - Eur. J.* **2009**, *15*, 9046–9057. (b) Paneque, M.; Poveda, M. L.; Santos, L. L.; Carmona, E.; Lledós, A.; Ujaque, G.; Mereiter, K. A Measureable Equilibrium between Iridium Hydride Alkylidene and Iridium Hydride Alkene Isomers. *Angew. Chem., Int. Ed.* **2004**, *43*, 3708–3711.

(22) Clot, E.; Chen, J.; Lee, D.-H.; Sung, S. Y.; Appelhans, L. N.; Faller, J. W.; Crabtree, R. H.; Eisenstein, O. Double Geminal C–H Activation and Reversible  $\alpha$ -Elimination in 2-Aminopyridine Iridium(III) Complexes: The Role of Hydrides and Solvent in Flattening the Free Energy Surface. *J. Am. Chem. Soc.* **2004**, *126*, 8795–8804.

(23) Schrock, R. R.; Seidel, S. W.; Mösch-Zanetti, N. C.; Shih, K.-Y.; O'Donoghue, M. B.; Davis, W. M.; Reiff, W. M. Synthesis and Decomposition of Alkyl Complexes of Molybdenum(IV) That Contain a  $[(\text{Me}_3\text{SiNCH}_2\text{CH}_2)_3\text{N}]^3$  Ligand. Direct Detection of  $\alpha$ -Elimination Processes That Are More than Six Orders of Magnitude Faster than  $\beta$ -Elimination Processes. *J. Am. Chem. Soc.* **1997**, *119*, 11876–11893.

(24) Campos, J.; Esqueda, A. C.; López-Serrano, J.; Sánchez, L.; Cossio, F. P.; de Cozar, A.; Álvarez, E.; Maya, C.; Carmona, E. A Cationic Rh(III) Complex That Efficiently Catalyzes Hydrogen Isotope Exchange in Hydrosilanes. *J. Am. Chem. Soc.* **2010**, *132*, 16765–16767.

(25) Brookhart, M.; Green, M. L. H.; Parkin, G. Agostic interactions in transition metal compounds. *Proc. Natl. Acad. Sci. U. S. A.* **2007**, *104*, 6908–6914.

(26) (a) Grabowski, S. J. What Is the Covalency of Hydrogen Bonding? *Chem. Rev.* **2011**, *111*, 2597–2625. (b) Saßmannshausen, J. Quo Vadis, agostic bonding? *Dalton Trans.* **2012**, *41*, 1919–1923. (c) Scherer, W.; McGrady, G. S. Agostic Interactions in  $d^0$  Metal Alkyl Complexes. *Angew. Chem., Int. Ed.* **2004**, *43*, 1782–1806. (d) van der Eide, E. F.; Yang, P.; Bullock, R. M. Isolation of Two Agostic Isomers of an Organometallic Cation: Different Structures and Colors. *Angew. Chem., Int. Ed.* **2013**, *52*, 10190–10194. (e) Dunlop-Brière, A. F.; Baird, M. C.; Budzelaar, P. H. M.  $[\text{Cp}_2\text{TiCH}_2\text{CHMe}(\text{SiMe}_3)]^+$ , an Alkyl–Titanium Complex Which (a) Exists in Equilibrium between a  $\beta$ -Agostic and a Lower Energy  $\gamma$ -Agostic Isomer and (b) Undergoes Hydrogen Atom Exchange between  $\alpha$ -,  $\beta$ -, and  $\gamma$ -Sites via a Combination of Conventional  $\beta$ -Hydrogen Elimination–Reinsertion and a Nonconventional CH Bond Activation Process Which Involves Proton Tunnelling. *J. Am. Chem. Soc.* **2013**, *135*, 17514–17527.

- (27) (a) Bruce, M. I. Organometallic chemistry of vinylidene and related unsaturated carbenes. *Chem. Rev.* **1991**, *91*, 197–257. (b) Bruneau, C.; Dixneuf, P. H. Metal Vinylidenes in Catalysis. *Acc. Chem. Res.* **1999**, *32*, 311–323. (c) Werner, H. Vinylidenerhodium complexes as promising tools for C–C coupling reactions. *Coord. Chem. Rev.* **2004**, *248*, 1693–1702. (d) Lynam, J. M. Recent Mechanistic and Synthetic Developments in the Chemistry of Transition-Metal Vinylidene Complexes. *Chem. - Eur. J.* **2010**, *16*, 8238–8247.
- (28) (a) Khushnutdinova, J. R.; Milstein, D. Metal–Ligand Cooperation. *Angew. Chem., Int. Ed.* **2015**, *54*, 12236–12273. (b) Milstein, D. Metal–ligand cooperation by aromatization–dearomatization as a tool in single bond activation. *Philos. Trans. R. Soc., A* **2015**, *373*, 20140189.
- (29) Arita, A. J.; Cantada, J.; Grotjahn, D. B.; Cooksy, A. L. Computational Study of the Extensive Role of Heterocyclic Ligands in Acetylene Hydration by a Bifunctional Organometallic Catalyst. *Organometallics* **2013**, *32*, 6867–6870.
- (30) (a) Álvarez, E.; Conejero, C.; Lara, P.; López, J. A.; Paneque, M.; Petronilho, A.; Poveda, M. L.; del Río, D.; Serrano, O.; Carmona, E. Rearrangement of Pyridine to Its 2-Carbene Tautomer Mediated by Iridium. *J. Am. Chem. Soc.* **2007**, *129*, 14130–14131. (b) Cristóbal, C.; Hernández, Y. A.; López-Serrano, J.; Paneque, M.; Petronilho, A.; Poveda, M. L.; Salazar, V.; Vattier, F.; Álvarez, E.; Maya, C.; Carmona, E. Reactivity Studies of Iridium Pyridylidenes [ $\text{Tp}^{\text{Me}_2}\text{Ir}(\text{C}_6\text{H}_5)_2(\text{C}(\text{CH}_3)_3\text{C}(\text{R})\text{NH})$ ] (R = H, Me, Ph). *Chem. - Eur. J.* **2013**, *19*, 4003–4020.
- (31) Crabtree, R. H. *The Organometallic Chemistry of the Transition Metals*; 5th ed.; John Wiley and Sons, 2009.
- (32) (a) Jaffart, J.; Cole, M. L.; Etienne, M.; Reinhold, M.; McGrady, J. E.; Maseras, F. C–H and C–C agostic interactions in cycloalkyl tris(pyrazolyl)boratoniobium complexes. *Dalton Trans.* **2003**, 4057–4064. (b) Jaffart, J.; Etienne, M.; Maseras, F.; McGrady, J. E.; Eisenstein, O. Equilibria between  $\alpha$ - and  $\beta$ -Agostic Stabilized Rotamers of Secondary Alkyl Niobium Complexes. *J. Am. Chem. Soc.* **2001**, *123*, 6000–6013. (c) Fryzuk, M. D.; Johnson, S. A.; Rettig, S. R. Reaction of  $[\text{P}_2\text{N}_2]\text{Ta}=\text{CH}_2(\text{Me})$  with Ethylene: Synthesis of  $[\text{P}_2\text{N}_2]\text{Ta}(\text{C}_2\text{H}_4)\text{Et}$ , a Neutral Species with a  $\beta$ -Agostic Ethyl Group in Equilibrium with an  $\alpha$ -Agostic Ethyl Group ( $[\text{P}_2\text{N}_2] = \text{PhP}(\text{CH}_2\text{SiMe}_2\text{NSiMe}_2\text{CH}_2)_2\text{PPh}$ ). *J. Am. Chem. Soc.* **2001**, *123*, 1602–1612. (d) Li, X.; Appelhans, L. N.; Faller, J. W.; Crabtree, R. H. Stoichiometric C–C Coupling Reactions in the Coordination Sphere of an Iridium(III) Alkyl. *Organometallics* **2004**, *23*, 3378–3387.
- (33) White, C.; Oliver, A. J.; Maitlis, P. M. Pentamethylcyclopentadienyl-rhodium and -iridium Complexes. Part VII. Mono-, Di-, and Tri- $\mu$ -Hydrido-complexes. *J. Chem. Soc., Dalton Trans.* **1973**, 1901–1907.
- (34) Clot, E.; Eisenstein, O.; Dubé, T.; Faller, J. W.; Crabtree, R. H. Interplay of Weak Interactions: An Iridium(III) System with an Agostic tert-Butyl but a Nonagostic Isopropyl Group. *Organometallics* **2002**, *21*, 575–580.
- (35) (a) Kang, J. W.; Maitlis, P. M. Pentamethylcyclopentadienyl-rhodium and -iridium complexes. V. Complexes with oxy-ligands and the exchange of methyl protons by deuterium under basic conditions. *J. Organomet. Chem.* **1971**, *30*, 127–133. (b) Vargaftik, M. N.; Struchkov, Y. T.; Yanovsky, A. I.; Maitlis, P. M. Synthesis and X-Ray Structure of  $\text{Cp}^*\text{Rh}(\text{III})$ -Molybdate Complexes Derived from Bis-(triphenylphosphineiminium) Mono- and Polymolybdates. *Mendeleev Commun.* **1993**, *3*, 247–249.
- (36) (a) Moseley, K.; Kang, J. W.; Maitlis, P. M. Pentamethylcyclopentadienyl-rhodium and -iridium halides. II. Reactions with mono-, di-, and triolefins. *J. Chem. Soc. A* **1970**, *17*, 2875–83. (b) Paneque, M.; Maitlis, P. M. Loss of pentamethylcyclopentadiene from pentamethylcyclopentadienylrhodium hydride complexes. *J. Chem. Soc., Chem. Commun.* **1989**, 105–106.
- (37) White, C.; Yates, A.; Maitlis, P. M.; Heinekey, D. M. ( $\eta^5$ -Pentamethylcyclopentadienyl)Rhodium and -Iridium Compounds. *Inorg. Synth.* **1992**, *29*, 228–234.
- (38) Brookhart, M.; Grant, B.; Volpe, A. F.  $[(3,5\text{-}(\text{CF}_3)_2\text{C}_6\text{H}_3)_4\text{B}][\text{H}(\text{OEt}_2)_2]^+$ : a convenient reagent for generation and stabilization of cationic, highly electrophilic organometallic complexes. *Organometallics* **1992**, *11*, 3920–3922.
- (39) Frisch, M. J.; Trucks, G. W.; Schlegel, H. B.; Scuseria, G. E.; Robb, M. A.; Cheeseman, J. R.; Scalmani, G.; Barone, V.; Mennucci, B.; Petersson, G. A.; Nakatsuji, H.; Caricato, M.; Li, X.; Hratchian, H. P.; Izmaylov, A. F.; Bloino, J.; Zheng, G.; Sonnenberg, J. L.; Hada, M.; Ehara, M.; Toyota, K.; Fukuda, R.; Hasegawa, J.; Ishida, M.; Nakajima, T.; Honda, Y.; Kitao, O.; Nakai, H.; Vreven, T.; Montgomery, J. A., Jr.; Peralta, J. E.; Ogliaro, F.; Bearpark, M. J.; Heyd, J.; Brothers, E. N.; Kudin, K. N.; Staroverov, V. N.; Keith, T.; Kobayashi, R.; Normand, J.; Raghavachari, K.; Rendell, A. P.; Burant, J. C.; Iyengar, S. S.; Tomasi, J.; Cossi, M.; Rega, N.; Millam, N. J.; Klene, M.; Knox, J. E.; Cross, J. B.; Bakken, V.; Adamo, C.; Jaramillo, J.; Gomperts, R.; Stratmann, R. E.; Yazyev, O.; Austin, A. J.; Cammi, R.; Pomelli, C.; Ochterski, J. W.; Martin, R. L.; Morokuma, K.; Zakrzewski, V. G.; Voth, G. A.; Salvador, P.; Dannenberg, J. J.; Dapprich, S.; Daniels, A. D.; Farkas, Ö.; Foresman, J. B.; Ortiz, J. V.; Cioslowski, J.; Fox, D. J. *Gaussian 09*, revision D.01; Gaussian, Inc.: Wallingford, CT, 2013.
- (40) (a) Perdew, J. P.; Burke, K.; Ernzerhof, M. Generalized Gradient Approximation Made Simple. *Phys. Rev. Lett.* **1996**, *77*, 3865–3868. (b) Perdew, J. P.; Burke, K.; Ernzerhof, M. Generalized Gradient Approximation Made Simple (Errata). *Phys. Rev. Lett.* **1997**, *78*, 1396.
- (41) Andrae, D.; Häußermann, U.; Dolg, M.; Stoll, H.; Preuß, H. Energy-adjusted *ab initio* pseudopotentials for the second and third row transition elements. *Theor. Chim. Acc.* **1990**, *77*, 123–141.
- (42) Marenich, A. V.; Cramer, C. J.; Truhlar, D. G. Universal Solvation Model Based on Solute Electron Density and on a Continuum Model of the Solvent Defined by the Bulk Dielectric Constant and Atomic Surface Tensions. *J. Phys. Chem. B* **2009**, *113*, 6378–6396.
- (43) Grimme, S.; Antony, J.; Ehrlich, S.; Krieg, H. A consistent and accurate *ab initio* parametrization of density functional dispersion correction (DFT-D) for the 94 elements H–Pu. *J. Chem. Phys.* **2010**, *132*, 154104.
- (44) Miloserdov, F. M.; McKay, D.; Muñoz, B. K.; Samouei, H.; Macgregor, S. A.; Grushin, V. V. Exceedingly Facile Ph–X Activation (X = Cl, Br, I) with Ruthenium(II): Arresting Kinetics, Autocatalysis, and Mechanisms. *Angew. Chem., Int. Ed.* **2015**, *54*, 8466–8470.
- (45) Miloserdov, F. M.; McMullin, C. L.; Belmonte, M. M. N.; Benet-Buchholz, J.; Bakhmutov, V. I.; Macgregor, S. A.; Grushin, V. V. The Challenge of Palladium-Catalyzed Aromatic Azidocarbonylation: From Mechanistic and Catalyst Deactivation Studies to a Highly Efficient Process. *Organometallics* **2014**, *33*, 736–752.